Short Title: Lipid complement of *Arabidopsis* leaf mitochondria

Defining the lipidome of Arabidopsis leaf mitochondria: Specific lipid complement and lipid biosynthesis capacity

Yi-Tse Liu[1], Jennifer Senkler[2], Cornelia Herrfurth[1,3], Hans-Peter Braun[2], Ivo Feussner[1,3,4,*]

[1]University of Goettingen, Albrecht-von-Haller-Institute for Plant Sciences, Department of Plant Biochemistry, 37077 Goettingen, Germany. [2]Leibniz Universität Hannover, Institute of Plant Genetics, Department of Plant Proteomics, 30419 Hannover, Germany. [3]University of Goettingen, Goettingen Center for Molecular Biosciences (GZMB), Service Unit for Metabolomics and Lipidomics, 37077 Goettingen, Germany. [4]University of Goettingen, Goettingen Center for Molecular Biosciences (GZMB), Department of Plant Biochemistry, 37077 Goettingen, Germany

***Author for correspondence:** Ivo Feussner, Justus-von-Liebig-Weg 11, 37077 Goettingen, Germany; Fax: +49-551-39-25749; Email: ifeussn@uni-goettingen.de

The authors responsible for distribution of materials integral to the findings presented in this article in accordance with the policy described in the Instructions for Authors (https://academic.oup.com/plphys/pages/General-Instructions) are Hans-Peter Braun, braun@genetik.uni-hannover.de and Ivo Feussner, ifeussn@uni-goettingen.de.

Author contributions: YL performed experiments including lipid analysis and pathway construction; JS performed proteomic analysis. YL, JS, CH, HB and IF analyzed the data. YL wrote the first draft of the manuscript. CH, HB and IF edited the manuscript. HB and IF designed and supervised the study. IF agrees to serve as the author responsible for contact and ensures communication.

Competing interests: Authors declare no competing interest.

Key words:

One sentence summary: The lipid landscape of plant mitochondria suggests that they are capable in generating several phospholipid classes with the assistant of membrane contact site-localized proteins.

Summary

Mitochondria are considered as power stations of the cell, playing critical roles in various biological processes such as energy conversion, stress responses and programmed cell death. To maintain the structural and functional integrities of mitochondria, it is crucial to achieve a defined membrane lipid composition between different lipid classes wherein specific proportions of individual lipid species are present. Although mitochondria are capable of self-synthesizing a few lipid classes, many phospholipids are synthesized in the endoplasmic reticulum and transferred to mitochondria via membrane contact sites, as mitochondria are excluded from the vesicular transportation pathway. However, knowledge on the capability of lipid biosynthesis in mitochondria and the precise mechanism of maintaining the homeostasis of mitochondrial lipids is still scarce. Here we describe the lipidome of mitochondria isolated from *Arabidopsis* leaves, including the molecular species of glycerolipids, sphingolipids and sterols to depict the lipid landscape of mitochondrial membranes. In addition, we define proteins involved in lipid metabolism by proteomic analysis. Proteins putatively localized to the membrane contact sites are proposed based on the proteomic results and online databases. Collectively, our results suggest that leaf mitochondria are capable, with the assistant of membrane contact site-localized proteins, in generating several lipid classes including phosphatidylethanolamines, cardiolipins, diacylgalactosylglycerols and free sterols. We anticipate our work to be a foundation to further investigate the functional roles of lipids and their involvement in biochemical reactions in plant mitochondria.

56 **Introduction**

57 Mitochondria are considered as semiautonomous organelles. According to a widely accepted
58 hypothesis, they descend from proteobacteria that have been engulfed to form an eukaryotic
59 cell. The two involved cells established an endosymbiosis (Gray et al., 1999). Mitochondria play
60 crucial roles in various cellular processes, including ATP generation, stress responses and
61 initiation of programmed cell death (Jacoby et al., 2012). The mitochondria of plant cells even
62 have extended functions, many of which are related to photosynthesis (Braun, 2020).
63 Mitochondria are enclosed by two membranes, the outer (OM) and the inner (IM) mitochondrial
64 membranes, that both require defined protein and lipid compositions to maintain their
65 functional integrity (Horvath and Daum, 2013; Michaud et al., 2017). The majority of the
66 mitochondrial proteins is encoded by the nuclear genome, synthesized in the cytoplasm and
67 post-translationally imported into the organelle. At the same time, a few proteins are encoded
68 by the mitochondrial genome and synthesized within the organelle. Recent studies have largely
69 broadened the knowledge of protein import in mitochondria, to the OM, the intermembrane
70 space, the IM and the matrix (Wiedemann and Pfanner, 2017). However, current understanding
71 of the biosynthesis and transport of lipids in plants, although fundamentally important
72 constituents of the mitochondria, is still very limited.

73 Wide varieties of lipid species compose biological membranes. According to the backbones of
74 the lipid molecules, they are classified into three main lipid categories – glycerolipids,
75 sphingolipids and sterols. To delineate the molecular species in this study, we later use the
76 taxonomy containing two colon-separated units for the numbers of carbons and double bonds
77 in the fatty acyl moiety, and an additional unit after a semicolon for the number of hydroxyl
78 groups (when present) (Liebisch et al., 2020). Mitochondrial membranes contain high amounts
79 of glycerophospholipids, such as phosphatidylcholine (PC) and phosphatidylethanolamine (PE),
80 but are low in sphingolipids and sterols (Moreau et al., 1974; Bligny and Douce, 1980). Most of
81 these lipids are produced in the ER and are sorted to mitochondria and other organelles
82 afterwards. Nevertheless, mitochondria have also their own capacity to generate some specific
83 lipid classes. For instance, cardiolipin (CL) is synthesized in the IM and is present exclusively in
84 mitochondria (Douce et al., 1972; Babiychuk et al., 2003). It plays essential roles in establishing
85 the cristae in the IM and in maintaining the mitochondrial ultrastructure. CL is formed through

86 the condensation of phosphatidylglycerol (PG) and diacylglycerol (DAG) and finally consists of
87 four acyl chains. The inner envelope of the plastid is the major site for generating PG molecules
88 (Müller and Frentzen, 2001). However, enzymes involved in PG biosynthesis are identified in
89 mitochondria as well, suggesting that mitochondria are capable of self-synthesizing PG and thus
90 CL (Babiychuk et al., 2003). In plants, the PG synthesizing enzymes,
91 phosphatidylglycerolphosphate (PGP) synthase and PGP phosphatase (PGPP), are associated
92 with mitochondria, and plastids; whereas CL synthase (CLS) localizes exclusively in the IM (Xu et
93 al., 2002; Katayama et al., 2004). Notably, although mitochondrial lipid biosynthesis is not the
94 major lipid source in plant cells, it is critical for certain organisms. In yeast, mitochondria are the
95 major supplier of PE (Horvath and Daum, 2013). They generate PE from phosphatidylserine (PS)
96 by phosphatidylserine decarboxylase (PSD). In *Arabidopsis*, three PSD enzymes have been
97 identified and PSD1 localizes in mitochondria, providing PE molecules *in situ* (Nerlich et al.,
98 2007). Reversely, some PS molecules are converted from PE through the base-exchange
99 pathway that substitutes the head groups of PE with serine molecules by PS synthase1, PSS1
100 (Yamaoka et al., 2011). While knowing mitochondria are capable of synthesizing PG, CL, PS and
101 PE, its competence toward other lipid classes is still poorly understood (Li-Beisson et al., 2013).

102 Lipid trafficking between ER, mitochondria and plastids is essential for mitochondrial membrane
103 biogenesis (Horvath and Daum, 2013; Michaud et al., 2017). Based on studies in yeast and
104 mammals, glycerophospholipid biosynthesis takes place at a distinct membrane stretch of the
105 ER, the mitochondria-associated membrane (MAM), wherein both ER and mitochondrial
106 proteins have been identified (Vance, 1990). Elevated activities of PE, PC and PS synthesizing
107 enzymes have been detected in purified yeast MAM. Moreover, this distinct membrane domain
108 seems to occur ubiquitously among plants and animal cells, suggesting its critical role during
109 evolution and in mediating lipid transfer between ER and mitochondria (Morré et al., 1971;
110 Staehelin, 1997; Achleitner et al., 1999; Michaud et al., 2016). Although mitochondria and
111 plastids work closely together in numerous pathways in plants, the lipid transport mechanism
112 between these two organelles is largely unknown. Nevertheless, a few studies have suggested
113 the relevance of lipid trafficking between these two organelles for survival, especially under
114 environmental stresses. During phosphate starvation, higher numbers of mitochondria – plastid
115 junctions are established (Jouhet et al., 2004). At the same time, drastic lipid remodeling of

116 mitochondria, plastids and plasma membrane arises. PC and PE are degraded to release the
117 phosphate residues for essential biological processes and the remaining molecules are recycled
118 to generate the typical plastidial glyceroglycolipid, digalactosyldiacylglycerol (DGDG). This
119 coincides with increased levels of CL in mitochondria isolated from *Arabidopsis* suspension cells
120 and calli (Michaud et al., 2017). In *Arabidopsis*, the protein complex involved in lipid trafficking
121 and tethering of the two mitochondrial membranes, the mitochondrial transmembrane
122 lipoprotein (MTL) complex, has been identified recently (Michaud et al., 2016). MTL is composed
123 of more than 200 subunits and it has been demonstrated that MTL promotes the translocation
124 of PE from IM to OM and the import of DGDG from plastids to mitochondria during phosphate
125 starvation. Furthermore, mutation of a newly identified MTL subunit, digalactosyldiacylglycerol
126 synthase suppressor 1 (DGS1), leads to alteration of plastidial and mitochondrial lipid
127 composition and deficiency in mitochondrial biogenesis (Li et al., 2019). The characterization of
128 the MTL complex provides an initial insight in understanding the mechanism of lipid trafficking
129 between mitochondria and plastids.

130 In this study, we aimed to characterize the lipid metabolism of *Arabidopsis* leaf mitochondria
131 and conducted an in-depth lipidomic analysis, providing the molecular species information of all
132 lipid categories including glycerolipids, sphingolipids and sterols to illustrate the lipid landscape
133 of mitochondria in *Arabidopsis* leaves. In combination with a proteomic approach, we intended
134 to specify the capacity of lipid biosynthesis and modification in plant mitochondria, defining lipid
135 species and classes that may be generated by mitochondria. We additionally propose putative
136 membrane contact site-localizing proteins and their roles in interorganelle communication. Our
137 results suggest that leaf mitochondria possess a defined lipid composition wherein specific lipid
138 molecular species appear. In addition, lipid trafficking between mitochondria, ER and plastids via
139 membrane contact sites provides assistance in maintaining the homeostasis of the lipid
140 composition in mitochondria.

141 **Results**

142 **Purity of mitochondrial fractions**

143 A combinatorial approach by lipidomics, proteomics and mining of online databases was applied
144 to investigate the lipid composition as well as the capacity of lipid metabolism of *Arabidopsis*

145 leaf mitochondria. Mitochondria were isolated by differential centrifugation combined with
146 Percoll density gradient centrifugation. To ensure and evaluate the purity of the mitochondrial
147 fractions, all samples were investigated by two-dimensional (2D) blue native (BN)/SDS PAGE and
148 by shotgun proteome analyses. Our mitochondrial fractions proved to be of good quality. The
149 two photosystems were not detectable on our 2D gels. Only trace amounts of the large subunit
150 from Rubisco, the most abundant protein in leaves, were visible in the leaf mitochondrial
151 fractions (L-mito) on BN/SDS gels, and the small subunit of Rubisco was barely visible (Fig. 1A,
152 Supplemental Fig. S1). Mitochondria isolated from dark-grown *Arabidopsis* cell culture (C-mito)
153 were investigated by the same procedure and used as an established control for contamination
154 from chloroplasts. The L-mito and C-mito fractions were highly similar (Fig. 1, Supplemental
155 Fig. S1). In addition, the purity of the mitochondrial fractions was investigated by label-free
156 quantitative shotgun proteomics. Building on the proteome data (Supplemental Tab. S1), the
157 proportion of mitochondria-localized proteins was calculated to be in the range of 87 to 94 %
158 (Fig. 1B, Supplemental Fig. S2). These results indicate that the mitochondrial fractions are of
159 high purity.

160

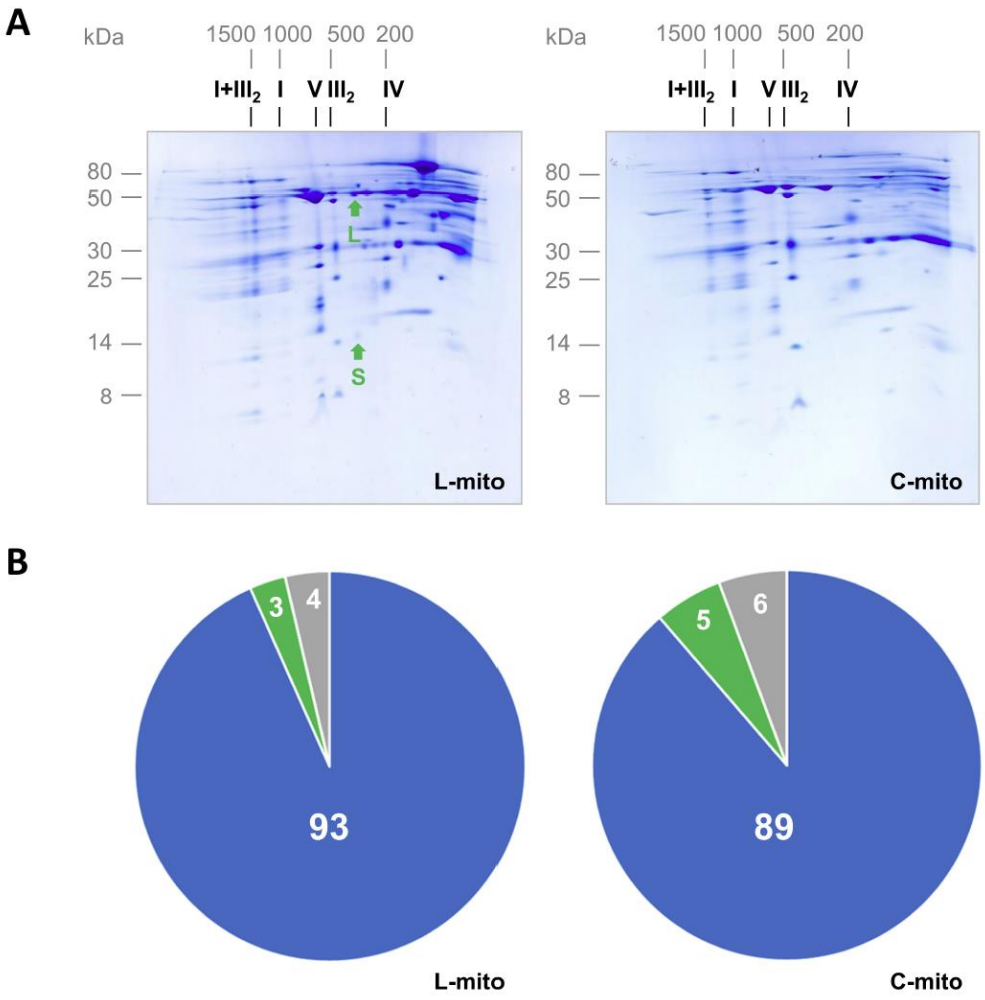

Figure 1. Purity of mitochondrial fractions. The purity of mitochondrial fractions was determined by 2D blue native / SDS PAGE **(A)** and by summed-up peptide intensities of subcellular compartments based on protein assignments as given by the Subcellular localization database for Arabidopsis proteins (SUBAcon; www.suba.live) **(B).**

A: Mitochondria were isolated from *Arabidopsis* leaves (L-mito) and cell cultures (C-mito). Proteins were separated by 2D Blue native PAGE and Coommassie-stained. Numbers on top and to the left of the 2D gels refer to the masses of standard protein complexes / proteins (in kDa), the roman numbers above the gels to the identity of OXPHOS complexes. $I+III_2$: supercomplex consisting of complex I and dimeric complex III; I: complex I; V: complex V; III_2: dimeric complex III; IV: complex IV. The small (S; 14.5 kDa) and the large (L; 53.5 kDa) subunit of Rubisco are indicated by green arrows. Biological replicates of the 2D gels and reference gels for mitochondrial and chloroplast fractions from *Arabidopsis* are shown in Fig. S1.

174 **PC, PE and CL are strongly enriched glycerolipids in plant leaf mitochondria**

175 Glycerolipids are the most abundant lipids not only in mitochondria but also generally in plant
176 tissues, accounting for more than 90 % of the overall lipids in leaves (Li-Beisson et al., 2013).
177 Glycerophospholipids are fundamental to all biological membranes, while glyceroglycolipids are
178 critical for photosynthetic membranes and localize mainly in plastids of vegetative tissues (Hölzl
179 and Dörmann, 2019). Therefore, a quantitative approach based on TLC-GC was applied on
180 determining the proportion of the major glycerolipid classes in L-TE and L-mito (Fig. 2). In L-TE,
181 glyceroglycolipids including monogalactosyldiacylglycerols (MGDG; 38.9 ± 1.1 %) and DGDG
182 (22.3 ± 3.8 %) contribute to the majority of the overall lipids; while glycerophospholipids, PC
183 (35.7 ± 6.0 %) and PE (37.2 ± 0.3 %), are the most abundant lipids in L-mito. CL accounts for 4.0
184 ± 0.9 % in the lipidome of L-mito; however, it was not detectable in L-TE because of its low
185 abundance in total cellular lipids. PG, as the precursor of CL, consists 5.6 ± 2.1 % of the overall
186 lipids in L-mito.

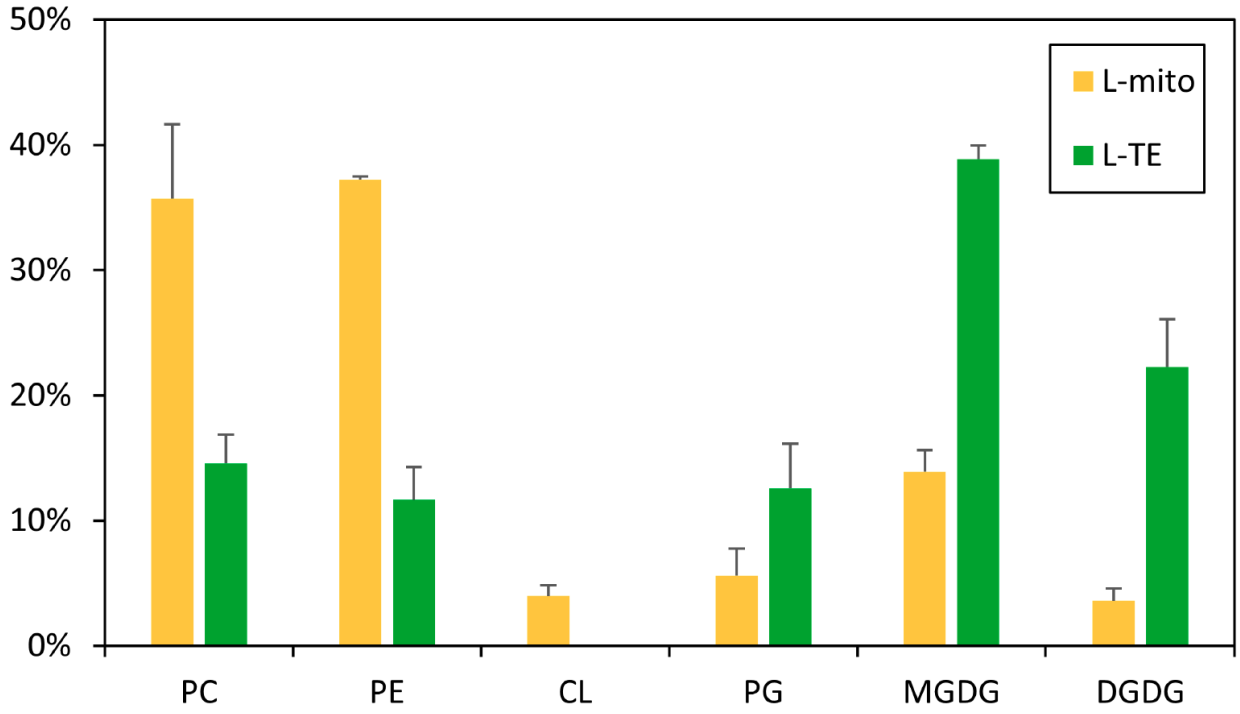

187

188 **Figure 2.** Lipid class profiles of purified mitochondria and total leaf extracts. Glycerolipids of leaf
189 total extract (L-TE) and mitochondria isolated from leaves (L-mito) were analyzed quantitatively
190 by TLC-GC approach. Data of L-TE represent mean values in mol % from three independent

191 experiments ± SD; data of L-mito represent mean values in mol % from two independent
192 experiments ± SEM. PC, phosphatidylcholine; PE, phosphatidylethanolamine; CL, cardiolipin; PG,
193 phosphatidylglycerol; MGDG, monogalactosyldiacylglycerol; DGDG, digalactosyldiacylglycerol.

194

195 **Specific molecular glycerolipid species are enriched in plant leaf mitochondria**

196 Glycerophospholipids are the most abundant lipids in mitochondria (Fig. 2) (Daum and Vance,
197 1997). The most abundant PC and PE molecular species in mitochondria with the acyl chains
198 18:2/18:3, 18:2/18:2 and 18:3/18:3 account for more than 60 % in both lipid classes (Fig. 3a;
199 Supplemental Tab. S2). The species 16:0/18:2, 16:0/18:3 of both lipid classes however were
200 depleted by about 50 % in this organelle in comparison to L-TE. PS (18:0/18:2) composes up to
201 38.3 % in L-mito with an increase of $2^{4.3}$ fold comparing to L-TE. The accumulation of this lipid
202 species was the most remarkable one that was even visible when the fatty acid profiles of the
203 different lipid classes were calculated from the molecular species data, showing an enrichment
204 of 18:0 in mitochondria on the expense of 16:0 (Supplemental Fig. S3). Together the main
205 molecular species of these three lipid classes have a C18/C18 acyl chain composition in
206 common.

a

PC (Mol%)	L-TE	L-mito	Mean	$Log_2(FC)$
* 16:0/16:0	0.0	0.0	0.0	
16:0/16:1	0.2	0.1	0.2	
** 16:0/18:1	2.1	1.0	1.5	-1.1
** 16:0/18:2	20.3	11.1	15.7	-0.9
** 16:0/18:3	17.7	12.9	15.3	-0.5
* 16:1/16:1	0.0	0.0	0.0	
16:1/18:0	0.0	0.0	0.0	
16:1/18:1	0.1	0.1	0.1	
16:1/18:2	0.5	0.5	0.5	0.0
16:1/18:3	0.6	0.6	0.6	0.0
18:0/18:0	0.0	0.0	0.0	
* 18:0/18:1	0.2	0.1	0.2	
** 18:0/18:2	1.8	1.0	1.4	-0.8
** 18:0/18:3	1.4	0.7	1.1	-0.9
18:1/18:1	0.4	0.4	0.4	
18:1/18:2	3.0	3.8	3.4	0.3
18:1/22:1	0.0	0.0	0.0	
* 18:1/18:3	2.7	3.7	3.2	0.4
** 18:2/18:2	13.6	18.7	16.1	0.5
** 18:2/18:3	20.6	29.4	25.0	0.5
18:2/20:1	0.1	0.1	0.1	
18:2/20:2	0.1	0.2	0.2	
18:2/22:0	0.0	0.0	0.0	
18:3/18:3	14.2	15.2	14.7	0.1
18:3/20:0	0.0	0.0	0.0	
18:3/20:1	0.1	0.1	0.1	
* 18:3/20:2	0.1	0.1	0.1	
* 18:3/22:0		0.0	0.0	

PE (Mol%)	L-TE	L-mito	Mean	$Log_2(FC)$
16:0/16:0	0.0	0.0	0.0	
16:0/16:1	0.1	0.3	0.2	
** 16:0/18:1	1.4	0.3	0.9	-2.3
** 16:0/18:2	31.1	8.0	19.6	-2.0
** 16:0/18:3	19.3	5.7	12.5	-1.8
16:1/18:0	0.0	0.0	0.0	
* 16:1/18:1	0.0	0.2	0.1	
** 16:1/18:2	0.4	0.2	0.3	
* 16:1/18:3	0.3	0.2	0.2	
18:0/18:1	0.1	0.0	0.0	
** 18:0/18:2	1.8	0.4	1.1	-2.3
** 18:0/18:3	1.1	0.4	0.8	-1.3
18:1/18:1	0.1	0.2	0.2	
* 18:1/18:2	3.1	2.4	2.7	-0.4
18:1/18:3	1.7	1.5	1.6	-0.2
** 18:2/18:2	12.7	25.2	18.9	1.0
** 18:2/18:3	17.5	40.3	28.9	1.2
* 18:2/20:0	0.2	0.1	0.2	
18:2/20:1	0.2	0.1	0.1	
* 18:2/20:2	0.2	0.3	0.3	
18:2/22:0	0.3	0.0	0.2	
18:2/24:0	0.2	0.0	0.1	
18:2/24:1	0.2	0.1	0.1	
** 18:3/18:3	7.0	13.6	10.3	0.9
18:3/20:0	0.2	0.0	0.1	
* 18:3/20:1	0.1	0.1	0.1	
18:3/20:2	0.1	0.1	0.1	
18:3/22:0	0.2	0.1	0.1	
18:3/24:0	0.1	0.1	0.1	
18:3/24:1	0.1	0.1	0.1	

PS (Mol%)	L-TE	L-mito	Mean	$Log_2(FC)$
16:0/16:0	0.9	1.1	1.0	0.2
16:0/16:1	0.6	0.3	0.4	
** 16:0/18:0	0.4	4.6	2.5	3.4
16:0/18:1	0.6	0.6	0.6	0.1
16:0/18:2	15.5	7.7	11.6	-1.0
** 16:0/18:3	26.4	5.7	16.0	-2.2
16:1/16:1		0.0	0.0	
16:1/18:0	0.2	0.2	0.2	
* 16:1/18:1		0.2	0.2	
16:1/18:2	0.8	0.1	0.4	
16:1/18:3	1.0	0.2	0.6	-2.1
* 18:0/18:0		0.2	0.2	
* 18:0/18:1	0.4	1.6	1.0	2.0
** 18:0/18:2	1.9	38.3	20.1	4.3
** 18:0/18:3	2.6	12.4	7.5	2.2
18:1/18:1		0.1	0.1	
18:1/18:2	1.1	0.9	1.0	-0.3
18:1/18:3	1.2	0.4	0.8	-1.4
18:2/18:2	0.7	0.7	0.7	0.0
* 18:2/18:3	3.3	0.8	2.0	-2.0
18:2/24:0	6.9	4.8	5.9	-0.5
18:2/24:1	11.2	9.6	10.4	-0.2
* 18:2/26:0	3.3	0.4	1.9	-3.0
* 18:2/26:1		2.0	2.0	
** 18:3/18:3	5.4	0.4	2.9	-3.8
* 18:3/24:0	9.8	3.6	6.7	-1.5
** 18:3/24:1	5.1	1.2	3.1	-2.1
18:3/26:0	0.2	0.1	0.1	
18:3/26:1	0.7	1.6	1.2	1.2

PI (Mol%)	L-TE	L-mito	Mean	$Log_2(FC)$
16:0/16:0	0.1	0.3	0.2	
16:0/16:1		0.5	0.5	
16:0/18:1	1.3	2.1	1.7	0.7
** 16:0/18:2	32.0	46.2	39.1	0.5
** 16:0/18:3	48.2	37.3	42.7	-0.4
16:1/16:1	0.5	0.0	0.3	
16:1/18:1		0.0	0.0	
16:1/18:2	0.8	0.3	0.6	-1.2
* 16:1/18:3	0.9	0.3	0.6	-1.5
18:0/18:0		0.1	0.1	
** 18:0/18:1		0.5	0.5	
* 18:0/18:2	1.0	2.3	1.6	1.2
18:0/18:3	2.2	2.1	2.1	0.0
** 18:1/18:1		0.2	0.2	
18:1/18:2	0.3	0.3	0.3	
18:1/18:3	1.0	0.8	0.9	-0.4
18:2/18:2	1.7	1.9	1.8	0.2
18:2/18:3	5.6	3.7	4.6	-0.6
* 18:3/18:3	4.6	1.2	2.9	-2.0

PIP_2 (Mol%)	L-TE	L-mito	Mean	$Log_2(FC)$
16:0/18:1	7.3	8.0	7.6	0.1
16:0/18:2	58.1	48.3	53.2	-0.3
16:0/18:3	27.2	34.6	30.9	0.3
** 18:1/18:2		4.7	4.7	
18:2/18:2	4.3	4.4	4.3	0.0
18:2/18:3	3.1		3.1	

PA (Mol%)	L-TE	L-mito	Mean	$Log_2(FC)$
** 16:0/16:0	0.0	1.3	0.6	5.3
** 16:0/16:1	0.2	0.4	0.3	
* 16:0/18:0	0.0	0.2	0.1	
16:0/18:1	1.0	3.1	2.1	1.6
** 16:0/18:2	16.2	22.2	19.2	0.5
* 16:0/18:3	18.1	20.7	19.4	0.2
** 16:1/16:1	0.0	0.1	0.0	
16:1/18:0	0.0	0.2	0.1	
** 16:1/18:1	0.0	0.2	0.1	
** 16:1/18:2	0.5	0.4	0.5	-0.5
* 16:1/18:3	0.5	0.3	0.4	
** 18:0/18:0		0.1	0.1	
** 18:0/18:1	0.1	0.2	0.1	
** 18:0/18:2	1.0	2.2	1.6	1.1
* 18:0/18:3	1.3	2.3	1.8	0.8
** 18:1/18:1	0.1	0.7	0.4	
* 18:1/18:2	2.3	3.0	2.7	0.4
18:1/18:3	2.4	2.4	2.4	0.0
** 18:2/18:2	14.9	12.2	13.5	-0.3
** 18:2/18:3	27.3	19.8	23.5	-0.5
** 18:3/18:3	14.0	8.1	11.1	-0.8

PG (Mol%)	L-TE	L-mito	Mean	$Log_2(FC)$
* 16:0/16:0	1.9	3.3	2.6	0.8
16:0/16:1	1.3	1.2	1.3	-0.1
** 16:0/18:0	0.2	0.7	0.4	
16:0/18:1	5.1	5.8	5.4	0.2
** 16:0/18:2	18.1	39.3	28.7	1.1
16:0/18:3	36.0	34.6	35.3	-0.1
16:1/16:1		0.2	0.2	
16:1/18:0	0.2	0.3	0.2	
16:1/18:1	1.0	0.9	0.9	-0.1
** 16:1/18:2	3.9	1.1	2.5	-1.8
** 16:1/18:3	29.6	5.9	17.7	-2.3
16:3/18:0	0.0	0.0	0.0	
16:3/18:1	0.0	0.0	0.0	
** 16:3/18:2	0.6	0.0	0.3	
* 16:3/18:3	0.3	0.0	0.1	
** 18:0/18:0		0.0	0.0	
* 18:0/18:1	0.0	0.2	0.1	
** 18:0/18:2	0.1	0.7	0.4	
** 18:0/18:3	0.1	0.4	0.2	
* 18:1/18:1	0.0	1.4	0.7	8.0
** 18:1/18:2	0.1	0.3	0.2	
** 18:1/18:3	0.1	0.3	0.2	
18:2/18:2	0.2	1.0	0.6	2.4
** 18:2/18:3	0.5	1.6	1.1	1.6
18:3/18:3	0.8	0.9	0.8	0.3

CL (Mol%)	L-mito
68:4	0.2
68:5	0.2
68:6	0.1
68:7	0.0
70:5	0.1
70:6	0.2
70:7	0.3
70:8	0.3
70:9	0.4
70:10	0.3
72:6	0.3
72:7	1.6
72:8	5.9
72:9	14.0
72:10	27.8
72:11	34.7
72:12	13.7

b

MGDG (Mol%)	L-TE	L-mito	Mean	$Log_2(FC)$
* 16:0/16:0	0.0	0.0	0.0	
16:0/16:1	0.0	0.0	0.0	
* 16:0/16:2	0.0	0.1	0.0	
** 16:0/16:3	0.1	0.1	0.1	
16:0/18:0	0.0	0.1	0.1	
** 16:0/18:1	0.6	1.4	1.0	1.1
16:0/18:2	0.5	0.9	0.7	0.7
* 16:0/18:3	0.8	2.3	1.6	1.5
16:1/16:1	0.0	0.0	0.0	
16:1/16:2	0.0	0.0	0.0	
16:1/16:3	0.1	0.1	0.1	
16:1/18:0	0.1	0.1	0.1	
* 16:1/18:1	0.8	0.5	0.7	-0.8
16:1/18:2	1.1	1.0	1.0	-0.1
* 16:1/18:3	1.3	0.9	1.1	-0.5
16:2/18:0	0.0	0.0	0.0	
16:2/18:1	0.4	0.4	0.4	
16:2/18:2	1.4	1.2	1.3	-0.2
** 16:2/18:3	3.6	2.6	3.1	-0.4
16:3/18:0	0.0	0.0	0.0	
* 16:3/18:1	0.3	0.2	0.3	
** 16:3/18:2	1.6	1.1	1.3	-0.6
** 16:3/18:3	63.8	52.1	57.9	-0.3
** 18:0/18:0	0.0	0.0	0.0	
* 18:0/18:1	0.0	0.1	0.0	
** 18:0/18:2	0.0	0.2	0.1	
** 18:0/18:3	0.1	0.3	0.2	
18:1/18:1	0.0	0.2	0.1	
18:1/18:2	0.1	0.2	0.1	
* 18:1/18:3	0.5	0.8	0.6	0.6
* 18:2/18:2	0.5	1.2	0.9	1.4
** 18:2/18:3	2.5	4.2	3.4	0.7
* 18:3/18:3	19.6	27.7	23.7	0.5

DGDG (Mol%)	L-TE	L-mito	Mean	$Log_2(FC)$
** 16:0/16:0	0.1	0.3	0.2	
16:0/16:1	0.0	0.0	0.0	
16:0/16:2	0.0	0.1	0.0	
16:0/16:3	0.0	0.1	0.0	
** 16:0/18:0	0.2	0.1	0.1	
16:0/18:1	1.3	1.2	1.2	-0.1
* 16:0/18:2	5.3	3.7	4.5	-0.5
16:0/18:3	11.8	11.4	11.6	-0.1
16:1/16:1		0.0	0.0	
16:1/16:2		0.0	0.0	
16:1/16:3		0.0	0.0	
16:1/18:0	0.0	0.0	0.0	
16:1/18:1	0.1	0.1	0.1	
16:1/18:2	0.2	0.2	0.2	
16:1/18:3	0.5	0.5	0.5	-0.1
16:2/18:0	0.0	0.1	0.0	
16:2/18:1	0.1	0.1	0.1	
16:2/18:2	0.2	0.3	0.3	
16:2/18:3	1.9	1.4	1.7	-0.4
16:3/18:0	0.0	0.1	0.1	
16:3/18:1	0.0	0.1	0.0	
* 16:3/18:2	0.2	0.4	0.3	
* 16:3/18:3	10.1	14.0	12.0	0.5
18:0/18:0		0.0	0.0	
** 18:0/18:1	0.0	0.1	0.1	
18:0/18:2	0.2	0.2	0.2	
18:0/18:3	0.8	1.0	0.9	0.4
18:1/18:1	0.0	0.0	0.0	
18:1/18:2	0.1	0.1	0.1	
** 18:1/18:3	0.8	1.0	0.9	0.3
18:2/18:2	0.4	0.4	0.4	
18:2/18:3	3.2	3.1	3.1	0.0
18:3/18:3	62.2	60.0	61.1	-0.1

c

DAG (Mol%)	L-TE	L-mito	Mean	$Log_2(FC)$
* 16:0/16:0	0.2	0.8	0.5	2.2
16:0/16:1	0.3	0.2	0.3	
16:0/18:0	0.9	0.7	0.8	-0.3
16:0/18:1	2.6	2.1	2.4	-0.3
** 16:0/18:2	29.8	20.4	25.1	-0.5
16:0/18:3	18.6	17.7	18.1	-0.1
16:0/20:0	0.1	0.1	0.1	
16:0/20:1	0.1	0.1	0.1	
16:0/22:0	0.1	0.1	0.1	
16:0/22:1	0.0	0.1	0.0	
16:0/24:0	0.1	0.2	0.1	
16:0/24:1	0.1	0.0	0.1	
16:1/16:1	0.0	0.1	0.1	
16:1/18:0	0.0	0.0	0.0	
16:1/18:1	0.2	0.3	0.2	
16:1/18:2	0.6	0.7	0.6	0.1
16:1/18:3	0.5	0.6	0.6	0.4
16:1/20:0	0.1	0.1	0.1	
16:1/20:1	0.1	0.1	0.1	
16:1/22:0	0.0	0.1	0.0	
16:1/22:1	0.1	0.1	0.1	
16:1/24:1	0.1	0.2	0.1	
18:0/18:0	0.8	0.4	0.6	-1.0
18:0/18:1	0.3	0.3	0.3	
* 18:0/18:2	2.9	2.0	2.5	-0.5
18:0/18:3	1.4	1.7	1.6	0.3
18:0/20:0	0.1	0.0	0.0	
18:0/20:1	0.0	0.0	0.0	
18:0/22:0	0.1	0.0	0.0	
18:0/22:1	0.1	0.0	0.1	
18:0/24:0	0.1	0.0	0.1	
18:0/24:1	0.0	0.0	0.0	

DAG (Mol%)	L-TE	L-mito	Mean	$Log_2(FC)$
* 18:1/18:1	0.3	0.6	0.5	0.9
* 18:1/18:2	2.4	3.2	2.8	0.4
18:1/18:3	2.7	2.8	2.7	0.0
18:1/20:0	0.1	0.0	0.1	
18:1/20:1	0.0	0.0	0.0	
18:1/22:0	0.0	0.0	0.0	
18:1/22:1	0.1	0.1	0.1	
18:1/24:0	0.0	0.0	0.0	
18:1/24:1	0.0	0.0	0.0	
18:2/18:2	10.1	9.5	9.8	-0.1
* 18:2/18:3	14.9	17.7	16.3	0.3
18:2/20:0	0.1	0.2	0.1	
18:2/20:1	0.3	0.2	0.2	
18:2/22:0	0.2	0.2	0.2	
18:2/22:1	0.3	0.2	0.2	
** 18:2/24:0	0.2	0.4	0.3	
* 18:2/24:1	0.1	0.2	0.2	
** 18:3/18:3	6.3	13.7	10.0	1.1
18:3/20:0	0.1	0.1	0.1	
18:3/20:1	0.2	0.2	0.2	
18:3/22:0	0.2	0.2	0.2	
18:3/22:1	0.1	0.1	0.1	
* 18:3/24:0	0.1	0.3	0.2	
* 18:3/24:1	0.1	0.2	0.1	
20:0/20:0	0.0	0.0	0.0	
20:0/20:1	0.0	0.0	0.0	
20:0/22:0	0.1	0.0	0.1	
20:0/22:1	0.0	0.0	0.0	
* 20:0/24:0	0.0	0.0	0.0	
* 20:0/24:1	0.1	0.0	0.0	
20:1/20:1	0.0	0.0	0.0	
20:1/22:0	0.0	0.0	0.0	
20:1/24:0	0.0	0.0	0.0	
20:1/24:1	0.0	0.0	0.0	
20:0/22:1	0.0	0.0	0.0	
22:0/22:0	0.0	0.1	0.0	
22:0/22:1	0.0	0.0	0.0	
* 22:0/24:0	0.0	0.2	0.1	
22:0/24:1	0.0	0.0	0.0	
22:1/22:1	0.0	0.0	0.0	
22:1/24:0	0.0	0.0	0.0	
22:1/24:1	0.1	0.1	0.1	
24:0/24:0	0.0	0.0	0.0	
24:0/24:1	0.0	0.0	0.0	
24:1/24:1		0.0	0.0	

207

208 **Figure 3.** Profiles of molecular glycerolipid species and the according fold changes between L-
209 mito and L-TE. Heat maps of (a) glycerophospholipids, (b) glyceroglycolipids and (c)
210 diacylglycerols illustrate the difference of species distribution based on LC-MS/MS analyses.
211 Each block represents one lipid class wherein the detected species are presented and
212 summarized to 100 %. Data represent mean values in mol % from three independent
213 experiments. Binary logarithm was applied when the mean values are higher than 0.5 to inspect
214 the fold changes (FC) between L-mito and L-TE. One and two asterisks (*, **) indicate p values <
215 0.05 and < 0.01, respectively, by Student's t-test. PC, phosphatidylcholine; PE,
216 phosphatidylethanolamine; PS: phosphatidylserine; PI: phosphatidylinositol; PA phosphatidic
217 acid; DAG: Diacylglycerol; CL, cardiolipin; PG, phosphatidylglycerol; MGDG,
218 monogalactosyldiacylglycerol; DGDG, digalactosyldiacylglycerol.

219

220 An important intermediate in glycerolipid metabolism is phosphatidic acid (PA), serving as
221 precursor or product for numerous glycerolipids including PC, PE, PG, phosphatidylinositol (PI)
222 and DAG. PA (16:0/18:2), PA (16:0/18:3) and PA (18:2/18:3) are the most abundant PA species in
223 both fractions, L-mito and L-TE. Notably, only a minor molecular PA species (16:0/16:0; 1.3 mol
224 %) accumulates preferentially in mitochondria with an enrichment of $2^{5.3}$ fold comparing to L-TE.
225 DAG as the other important lipid intermediate displays a higher complexity in its species profile.
226 DAG (16:0/18:2), DAG (16:0/18:3), DAG (18:2/18:3) and DAG (18:3/18:3) build a substantial
227 amount (>65 mol %) of the DAG profile in L-mito (Fig. 3c). As in case of PA, only the minor DAG
228 species (16:0/16:0) shows a $2^{2.2}$ fold increase in L-mito compared to L-TE.

229 PG is formed from PA in the envelopes of plastids and mitochondria and serves as precursor for
230 the mitochondrial lipid CL (Babiychuk et al., 2003). Hydrolysis and condensation of PG lead to
231 the formation of DAG and CL correspondingly. PG (16:0/18:2) and PG (16:0/18:3) are the major
232 species in L-mito, but only the former species is enriched in mitochondria ($2^{1.1}$ fold). In addition,
233 unsaturated PG species are significantly enriched in L-mito, which contribute to the structures of
234 the down-stream CL molecules. CL (72:10) and CL (72:11), composed of 18:2 and 18:3 acyl
235 chains, are the most abundant CL (Fig. 3a).

236 Glycerophospholipids serve not only as membrane building blocks but are also important
237 precursors for signaling molecules in the cell. PI, phosphatidylinositol monophosphate (PIP) and
238 phosphatidylinositol bisphosphate (PIP_2) exert regulatory functions in cell development and
239 polarity determination (Heilmann, 2016). In L-mito, molecular species with 16:0/18:2 and
240 16:0/18:3 acyl chains compose up to 80 % of PI and PIP_2; yet PIP was not detectable in L-mito.
241 PI (16:0/16:1) and PI (18:0/18:1) were only detectable in the mitochondrial extracts, and
242 PI (18:0/18:2) is significantly enriched in L-mito for $2^{1.2}$ fold in comparison to L-TE (Fig. 3a). On
243 the other hand, we obtained higher signals of PIP_2 (18:1/18:2) in L-mito.

244 Glyceroglycolipids carry carbohydrate residues as their head groups; for instance, the galactose-
245 containing lipids, MGDG and DGDG contain one and two galactoses, respectively (Hölzl and
246 Dörmann, 2019). MGDG (16:3/18:3) and DGDG (18:3/18:3) are the major components of the
247 overall glyceroglycolipids in both L-TE and L-mito (Fig. 3b). The amount of MGDG (16:0/18:3)
248 and MGDG (18:2/18:2) are specifically elevated in L-mito for $2^{1.5}$ and $2^{1.4}$ folds, respectively,
249 compared to L-TE. In contrast, the species MGDG (16:1/18:1) and MGDG (16:3/18:2) are
250 significantly decreased in L-mito. In summary, the major mitochondrial lipids PC, PE, PS and CL
251 consist primarily of C18/C18 species, while PI, PIP2 and PG consist primarily of C16/C18 species
252 and the lipid precursors DAG and PA resemble a mixture of both backbones.

253 **Proteomic analyses provides insights into the leaf mitochondrial glycerolipid metabolism**
254 **capacity**

255 To further analyze the proteome of the mitochondrial fractions, their protein composition was
256 investigated for enzymes from lipid metabolism. Subsequently, their biological function and the
257 subcellular localization were retrieved from The Arabidopsis Information Resource (TAIR) and
258 the Subcellular localization database for Arabidopsis proteins (SUBAcon) databases
259 (Supplemental Fig. S4).

260 About 40 proteins involved in the biosynthesis and modification of fatty acids and more complex
261 lipids were identified in mitochondrial extracts (Supplemental Tab. S3). Four enzymes from
262 glycerophospholipid metabolism were detected in all mitochondrial fractions (Fig. 4). Two
263 glycerol-3-phosphate dehydrogenases were identified (SDP6 and GPDHp), being involved in an
264 early step of glycerophospholipid biosynthesis. Phosphoethanolamine cytidylyltransferase

265 (PECT) was detected in our study by similar abundances in the L-mito and C-mito samples. CL is
266 synthesized after the condensation of PG and CDP-DAG by CL synthase (CLS) or after the
267 transacylation of monolyso-CL by monolysocardiolipin acyltransferase (LCLAT or Tafazzin)(Xu et
268 al., 2006). CLS and Tafazzin were identified in the shotgun proteomic analysis in this study with a
269 higher abundance in C-mito compared to L-mito. PG is synthesized from PA via CDP-DAG by
270 phosphatidylglycerophosphate synthase 1 (PGP1) (Xu et al., 2002) and it was only detected in C-
271 mito samples. Phosphatidylserine decarboxylase 1 (PSD1) synthesizes PE by decarboxylating the
272 headgroup of PS (Birner et al., 2001; Nerlich et al., 2007). Again in our study PSD1 was only
273 detected in C-mito samples. Interestingly PE and PC can be interconverted into each other via
274 PA and the detected phospholipase Dα1 (PLDα1) enzyme activity. PLDα1 was preferentially
275 found in C-mito samples. PIP and PIP_2 can be degraded by *myo*-inositol polyphosphate 1-
276 phosphatase (SAL1). Although many enzymes involved in phosphoinositide metabolism have
277 been annotated to localize in mitochondria, only SAL1 was identified in our approach in the C-
278 mito samples.

a Glycerophospholipid metabolism

L-mito	C-mito	Locus	Name	Function
		AT2G38670	PECT1	Ethanolamine-phosphatecytidylyltransferase
		AT2G39290	*PGP1*	CDP-DAG-G3P3-phosphatidyltransferase1
		AT3G10370	SDP6	Glycerol-3-phosphatedehydrogenase
		AT3G15730	PLDα1	PhospholipaseDalpha1
		AT4G04870	CLS	Cardiolipinsynthase
		AT4G16700	PSD1	PSdecarboxylaseproenzyme1
		AT1G78690	LCLAT	Monolysocardiolipinacyltransferase
		AT5G40610	GPDHp	Glycerol-3-phosphatedehydrogenase

b Glyceroglycolipid metabolism

L-mito	C-mito	Locus	Name	Function
		AT4G33030	*SQD1*	Sulfoquinovosyldiacylglycerol1

c Phosphoinositide metabolism

L-mito	C-mito	Locus	Name	Function
		AT5G63980	SAL1	Inositolpolyphosphate1-phosphatase

279

280 **Figure 4.** Mitochondrial localized proteins that are related to glycerolipid biosynthesis. (a)
281 Glycerophospholipid, (b) glyceroglycolipid and (c) phosphoinositide metabolism. Proteins
282 identified and/or localized in mitochondria were labeled (i) blue: proteins identified in the
283 proteomic analysis of this study and also predicted to localize in mitochondria, (ii) green:
284 proteins identified in the proteomic analysis of this study in mitochondria but predicted to

285 localize in other organelles, (iii) bold font: exclusively localized in mitochondria and (iv) italic
286 font: only identified in one of the mitochondrial populations. Heat maps visualize the protein
287 abundance of three independent experiments of mitochondria purified from leaves and cell
288 cultures. Predicted protein localization was based on The Arabidopsis Information Resource
289 (TAIR; www.arabidopsis.org) and the Subcellular localization database for Arabidopsis proteins
290 (SUBAcon; www.suba.live).

291

292 The biosynthesis of glyceroglycolipids takes place in the plastids envelopes by MGDG and DGDG
293 synthases (MGDs and DGDs), respectively (Hölzl and Dörmann, 2019). MGDG is generated by
294 adding a galactose head group to DAG; subsequent addition of another galactose by DGD1
295 generates DGDG. The detected specific species profiles of mitochondrial glyceroglycolipids may
296 suggest at least for a specific transport from plastids to mitochondria (Fig. 3b). The sulfolipid
297 SQDG is synthesized in two steps. Uridine diphosphate (UDP)-glucose is first combined with a
298 sulfite by UDP-sulfoquinovose synthase 1 (SQD1), followed by transferring the sulfoquinovose
299 head group to DAG and thus forms SQDG. Although SQD1 was identified in the C-mito samples
300 in this study, we did not detect SQDG lipids in any of the mitochondrial samples. Together we
301 could exclusively localize three biosynthetic steps to mitochondria: (i) CLS and catalyzing the
302 formation of CL as well as (ii) PSD1 and (iii) PECT1 facilitating PE formation.

303 **Specific molecular sphingolipid and sterol species suggest a function in mitochondria**

304 Sphingolipids and sterols are important modulators of membrane microdomains and play
305 critical roles in regulating the balance between cell survival and apoptosis. Therefore we profiled
306 next their mitochondrial compositions. For sphingolipids both simple and complex sphingolipids
307 were measured, including long-chain bases (LCB), phosphorylated LCB (LCB-P), ceramides (Cer),
308 glucosylceramides (GlcCer) and glycosyl inositol phosphoceramides (GIPC) (Fig. 5). All
309 sphingolipids have LCBs, 18-carbon amino-alcohols, as their backbones. Phytosphingosine
310 (18:0;3), hosting three hydroxyl groups, is the most abundant free LCB in both L-mito and L-TE
311 (Fig. 5a). However, dihydrosphingosine (18:0;2) is highly enriched in L-mito as well as
312 phosphorylated dihydrosphingosine (18:0;2-P), which is the major component in the LCB-P pool
313 of L-mito (64.7 %). LCBs can be further *N*-acylated to generate Cer, the basic structure of

complex sphingolipid classes. Addition of glucoses to Cer generates GlcCer, following sequential extension of phosphoinositol, hexose and/or hexose derivatives generate series of GIPCs. Series 0, A and B GIPCs carry one, two and three additional hexoses on the head groups of inositol phosphoceramides, respectively (Cacas et al., 2012; Haslam and Feussner, 2022). Similar to LCB and LCB-P, only specific species were enriched in L-mito (Fig. 5b): Cer (18:0;3/24:0;1), GlcCer (18:1;2/24:1;1) and series A hexose-carrying GIPC (H-GIPC) (18:1;3/24:1;1). Remarkably, GIPCs were only detectable in mitochondrial samples (both L-mito and C-mito) in our approach. However, proteins related to sphingolipid metabolism were neither identified in plant mitochondria via proteomic analyses, nor retrieved from online databases.

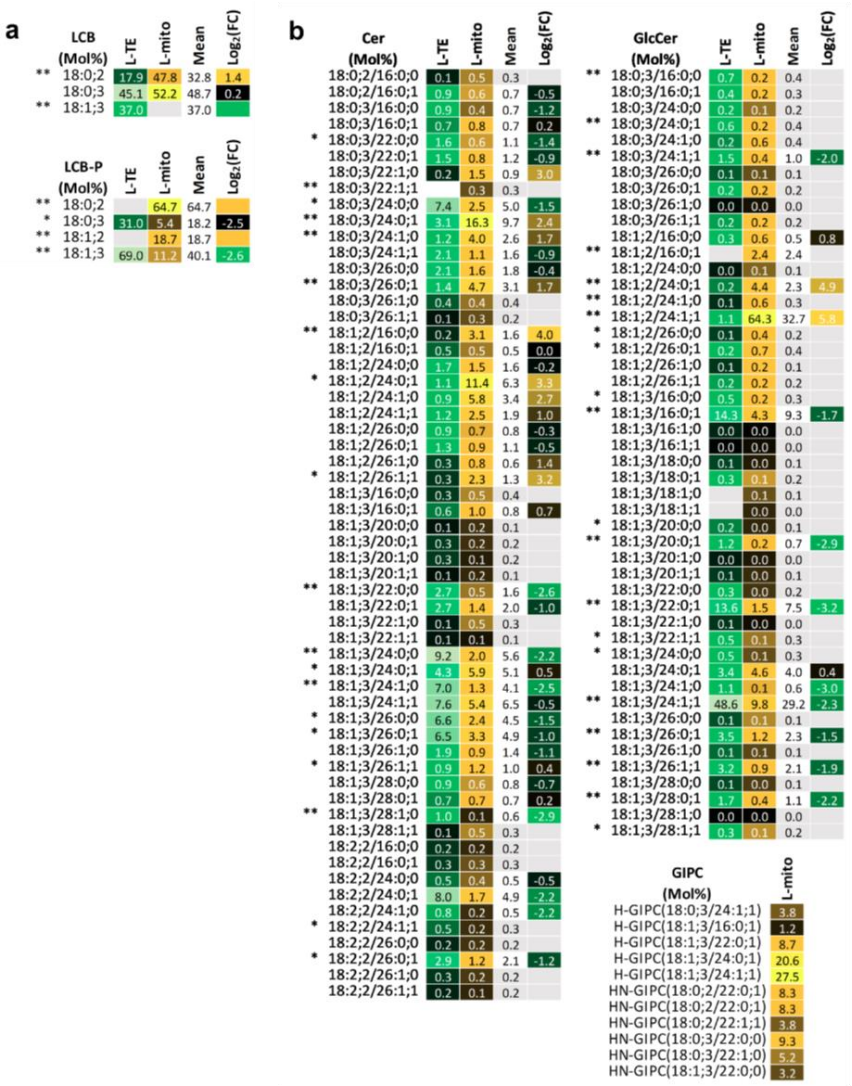

a

	LCB (Mol%)	L-TE	L-mito	Mean	Log_2(FC)
**	18:0;2	17.9	47.8	32.8	1.4
	18:0;3	45.1	52.2	48.7	0.2
**	18:1;3	37.0		37.0	

	LCB-P (Mol%)	L-TE	L-mito	Mean	Log_2(FC)
**	18:0;2		64.7	64.7	
*	18:0;3	31.0	5.4	18.2	-2.5
**	18:1;2		18.7	18.7	
**	18:1;3	69.0	11.2	40.1	-2.6

b

	Cer (Mol%)	L-TE	L-mito	Mean	Log_2(FC)
	18:0;2/16:0;0	0.1	0.5	0.3	
	18:0;2/16:0;1	0.9	0.6	0.7	-0.5
	18:0;3/16:0;0	0.9	0.4	0.7	-1.2
	18:0;3/16:0;1	0.7	0.8	0.7	0.2
*	18:0;3/22:0;0	1.6	0.6	1.1	-1.4
	18:0;3/22:0;1	1.5	0.8	1.2	-0.9
	18:0;3/22:1;0	0.2	1.5	0.9	3.0
**	18:0;3/22:1;1		0.3	0.3	
*	18:0;3/24:0;0	7.4	2.5	5.0	-1.5
**	18:0;3/24:0;1	3.1	16.3	9.7	2.4
**	18:0;3/24:1;0	1.2	4.0	2.6	1.7
	18:0;3/24:1;1	2.1	1.1	1.6	-0.9
	18:0;3/26:0;0	2.1	1.6	1.8	-0.4
**	18:0;3/26:0;1	1.4	4.7	3.1	1.7
	18:0;3/26:1;0	0.4	0.4	0.4	
	18:0;3/26:1;1	0.1	0.3	0.2	
**	18:1;2/16:0;0	0.2	3.1	1.6	4.0
	18:1;2/16:0;1	0.5	0.5	0.5	0.0
	18:1;2/24:0;0	1.7	1.5	1.6	-0.2
*	18:1;2/24:0;1	1.1	11.4	6.3	3.3
	18:1;2/24:1;0	0.9	5.8	3.4	2.7
	18:1;2/24:1;1	1.2	2.5	1.9	1.0
	18:1;2/26:0;0	0.9	0.7	0.8	-0.3
	18:1;2/26:0;1	1.3	0.9	1.1	-0.5
	18:1;2/26:1;0	0.3	0.8	0.6	1.4
*	18:1;2/26:1;1	0.3	2.3	1.3	3.2
	18:1;3/16:0;0	0.3	0.5	0.4	
	18:1;3/16:0;1	0.6	1.0	0.8	0.7
	18:1;3/20:0;0	0.1	0.2	0.1	
	18:1;3/20:0;1	0.3	0.2	0.2	
	18:1;3/20:1;0	0.3	0.1	0.2	
	18:1;3/20:1;1	0.1	0.2	0.1	
**	18:1;3/22:0;0	2.7	0.5	1.6	-2.6
	18:1;3/22:0;1	2.7	1.4	2.0	-1.0
	18:1;3/22:1;0	0.1	0.5	0.3	
	18:1;3/22:1;1	0.1	0.1	0.1	
**	18:1;3/24:0;0	9.2	2.0	5.6	-2.2
*	18:1;3/24:0;1	4.3	5.9	5.1	0.5
**	18:1;3/24:1;0	7.0	1.3	4.1	-2.5
	18:1;3/24:1;1	7.6	5.4	6.5	-0.5
*	18:1;3/26:0;0	6.6	2.4	4.5	-1.5
*	18:1;3/26:0;1	6.5	3.3	4.9	-1.0
	18:1;3/26:1;0	1.9	0.9	1.4	-1.1
*	18:1;3/26:1;1	0.9	1.2	1.0	0.4
	18:1;3/28:0;0	0.9	0.6	0.8	-0.7
	18:1;3/28:0;1	0.7	0.7	0.7	0.2
**	18:1;3/28:1;0	1.0	0.1	0.6	-2.9
	18:1;3/28:1;1	0.1	0.5	0.3	
	18:2;2/16:0;0	0.2	0.2	0.2	
	18:2;2/16:0;1	0.3	0.3	0.3	
	18:2;2/24:0;0	0.5	0.4	0.5	-0.5
	18:2;2/24:0;1	8.0	1.7	4.9	-2.2
	18:2;2/24:1;0	0.8	0.2	0.5	-2.2
*	18:2;2/24:1;1	0.5	0.2	0.3	
	18:2;2/26:0;0	0.2	0.2	0.2	
*	18:2;2/26:0;1	2.9	1.2	2.1	-1.2
	18:2;2/26:1;0	0.3	0.2	0.2	
	18:2;2/26:1;1	0.2	0.1	0.2	

	GlcCer (Mol%)	L-TE	L-mito	Mean	Log_2(FC)
**	18:0;3/16:0;0	0.7	0.2	0.4	
	18:0;3/16:0;1	0.4	0.2	0.3	
	18:0;3/24:0;0	0.2	0.1	0.2	
**	18:0;3/24:0;1	0.6	0.2	0.4	
	18:0;3/24:1;0	0.2	0.6	0.4	
**	18:0;3/24:1;1	1.5	0.4	1.0	-2.0
	18:0;3/26:0;0	0.1	0.1	0.1	
	18:0;3/26:0;1	0.2	0.2	0.2	
	18:0;3/26:1;0	0.0	0.0	0.0	
	18:0;3/26:1;1	0.2	0.2	0.2	
	18:1;2/16:0;0	0.3	0.6	0.5	0.8
**	18:1;2/16:0;1		2.4	2.4	
	18:1;2/24:0;0	0.0	0.1	0.1	
**	18:1;2/24:0;1	0.2	4.4	2.3	4.9
**	18:1;2/24:1;0	0.1	0.6	0.3	
**	18:1;2/24:1;1	1.1	64.3	32.7	5.8
*	18:1;2/26:0;0	0.1	0.4	0.2	
*	18:1;2/26:0;1	0.2	0.7	0.4	
	18:1;2/26:1;0	0.1	0.2	0.1	
	18:1;2/26:1;1	0.2	0.2	0.2	
*	18:1;3/16:0;0	0.5	0.2	0.3	
**	18:1;3/16:0;1	14.3	4.3	9.3	-1.7
	18:1;3/16:1;0	0.0	0.0	0.0	
	18:1;3/16:1;1	0.0	0.0	0.0	
	18:1;3/18:0;0	0.1	0.0	0.1	
	18:1;3/18:0;1	0.3	0.1	0.2	
	18:1;3/18:1;0		0.1	0.1	
	18:1;3/18:1;1		0.0	0.0	
*	18:1;3/20:0;0	0.2	0.0	0.1	
**	18:1;3/20:0;1	1.2	0.2	0.7	-2.9
	18:1;3/20:1;0	0.0	0.0	0.0	
	18:1;3/20:1;1	0.1	0.0	0.1	
	18:1;3/22:0;0	0.3	0.0	0.2	
**	18:1;3/22:0;1	13.6	1.5	7.5	-3.2
	18:1;3/22:1;0	0.1	0.0	0.0	
*	18:1;3/22:1;1	0.5	0.1	0.3	
*	18:1;3/24:0;0	0.5	0.1	0.3	
	18:1;3/24:0;1	3.4	4.6	4.0	0.4
	18:1;3/24:1;0	1.1	0.1	0.6	-3.0
**	18:1;3/24:1;1	48.6	9.8	29.2	-2.3
	18:1;3/26:0;0	0.1	0.1	0.1	
**	18:1;3/26:0;1	3.5	1.2	2.3	-1.5
	18:1;3/26:1;0	0.1	0.1	0.1	
**	18:1;3/26:1;1	3.2	0.9	2.1	-1.9
	18:1;3/28:0;0	0.1	0.0	0.1	
**	18:1;3/28:0;1	1.7	0.4	1.1	-2.2
	18:1;3/28:1;0	0.0	0.0	0.0	
*	18:1;3/28:1;1	0.3	0.1	0.2	

GIPC (Mol%)	L-mito
H-GIPC(18:0;3/24:1;1)	3.8
H-GIPC(18:1;3/16:0;1)	1.2
H-GIPC(18:1;3/22:0;1)	8.7
H-GIPC(18:1;3/24:0;1)	20.6
H-GIPC(18:1;3/24:1;1)	27.5
HN-GIPC(18:0;2/22:0;1)	8.3
HN-GIPC(18:0;2/22:0;1)	8.3
HN-GIPC(18:0;2/22:1;1)	3.8
HN-GIPC(18:0;3/22:0;0)	9.3
HN-GIPC(18:0;3/22:1;0)	5.2
HN-GIPC(18:1;3/22:0;0)	3.2

Figure 5. Profiles of molecular sphingolipid species, the according fold changes between L-mito and L-TE and general sphingolipid biosynthesis pathway in combination with mitochondrial

326 enriched lipids. Heat maps of (a) long chain bases, long chain base-phosphates and (b) complex
327 sphingolipids illustrate the difference of species distribution based on LC-MS/MS analyses. Each
328 block represents one lipid class wherein the detected species are presented and summarized to
329 100 %. Data represent mean values in mol % from three independent experiments. Binary
330 logarithm was applied when the mean values are higher than 0.5 to inspect the fold changes
331 (FC) between L-mito and L-TE. One and two asterisks (*, **) indicate p values < 0.05 and < 0.01,
332 respectively, by Student's t-test.

333

334 The common structure of sterols is a four-ring system, cyclopentanoperhydrophenanthrene,
335 with possible conjugation of hydroxyl groups and acyl chains. In plants, a complex mixture of
336 sterols can be found, including brassicasterol, campesterol, cholesterol, sitosterol and
337 stigmasterol (Cacas et al., 2012). Campesterol was identified as major free sterol with 61.7 % in
338 L-mito (Fig. 6). From the group of steryl glycosides cholesteryl and isofucosteryl glycoside
339 accumulated preferentially in L-mito. Considering SE, 16:0 and 18:0 containing cholesteryl esters
340 were enriched $2^{3.4}$ and $2^{5.3}$ folds, respectively, in L-mito. For ASG however the situation was
341 blurred. DWF1 was the only protein related to sterol metabolism that we identified in plant
342 mitochondria via proteomic analyses. In summary, we observed an accumulation of GIPCs and
343 free campersterol in leaf mitochondria.

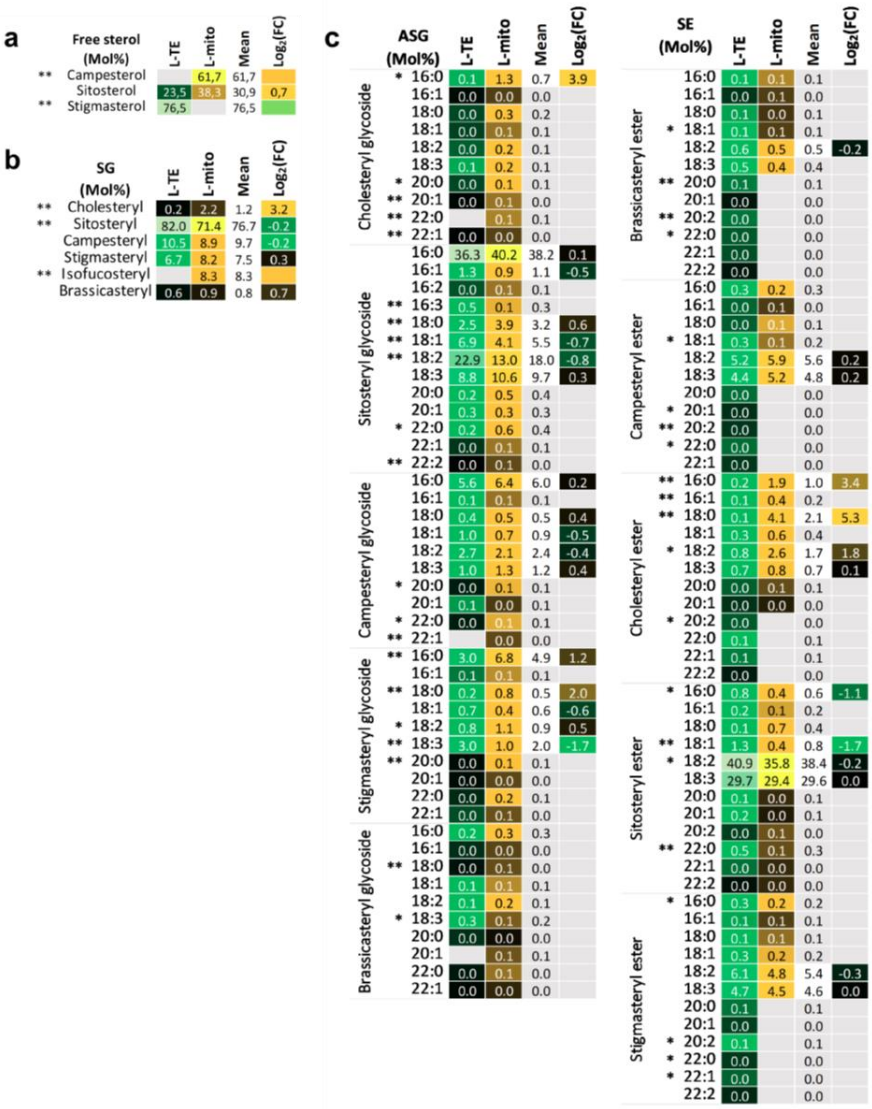

Figure 6. Profiles of molecular sterol species, the according fold changes between L-mito and L-TE and general sterol biosynthesis pathway in combination of mitochondrial localized proteins and enriched lipids. Heat maps of (a) free sterols (b) steryl glycosides (SG) and (c) acylated steryl glycosides (ASG) and steryl esters (SE) illustrate the difference of species distribution based on LC-MS/MS analyses. Each block represents one lipid class wherein the detected species are presented and summarized to 100 %. Data represent mean values in mol % from three independent experiments. Binary logarithm was applied when the mean values are higher than 0.5 to inspect the fold changes (FC) between L-mito and L-TE. One and two asterisks (*, **) indicate p values < 0.05 and < 0.01, respectively, by Student's t-test.

354 Mitochondria harbor various additional metabolic pathways for the synthesis of lipophilic
355 molecules. More than 20 fatty acid biosynthesis-related proteins were identified in our
356 mitochondrial proteome (Supplemental Fig. S5). They contribute to the synthesis of lipoic acid,
357 ubiquinone and other terpenoid-quinones. Abundance, function and predicted localization of
358 these proteins are specified in Supplemental Tab. S1 and S3.

359 **Lipid molecules can be imported by mitochondria**

360 Transport of DGDG from plastids to mitochondria and reallocation of PE from IM to OM via the
361 MTL complex have been demonstrated under phosphate-depleting conditions (Michaud et al.,
362 2016). The MTL complex has more than 200 subunits and 11 have been verified to associate
363 physically with the core subunits, Mic60 and Tom40, as previously shown by immunoblotting
364 (Michaud et al., 2016; Li et al., 2019). In our mitochondrial proteome, 186 of the subunits (87 %)
365 were identified including all the 11 verified ones (Fig. 7). The newly identified MTL subunit,
366 DGS1, which links mitochondrial protein to lipid transport, is present in all mitochondrial
367 extracts.

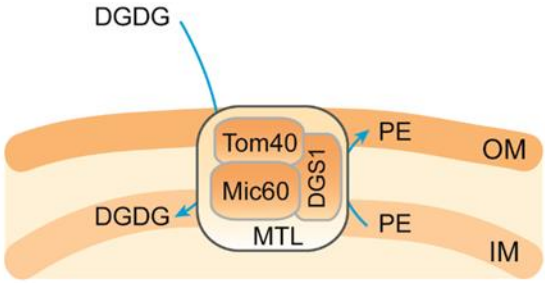

L-mito	C-mito	Locus	Name	Description
		AT1G06530	PMD2	Peroxisomal and mitochondrial division factor 2
		AT1G27390	TOM20-2	Translocase of outer membrane 20 kDa subunit 2
		AT2G37410	TIM17-2	Translocase inner membrane subunit 17-2
		AT2G42210	B14.7	Mitochondrial import inner membrane translocase subunit family protein
		AT3G20000	TOM40	Translocase of the outer mitochondrial membrane 40 kDa
		AT3G27080	TOM20-3	Translocase of outer membrane 20 kDa subunit 3
		AT4G39690	Mic60	Mitochondrial contact site and cristae organizing system subunit
		AT5G12290	DGS1	dgd1 suppressor 1
		AT5G13430	RISP	Ubiquinol-cytochrome c reductase iron-sulfur subunit
		AT5G40930	TOM20-4	Translocase of outer membrane 20 kDa subunit 4
		ATMG00160	COX2	Cytochrome oxidase 2

L-mito	C-mito	Locus	Name	Function
		AT3G19820	DWF1	Delta(24)-sterolreductase

368

369

370 **Figure 7.** MTL complex-associated proteins in mitochondria. Our proteomic analyses covered
371 186 of the 214 hypothetical subunits in the MTL complex (listed in Supplemental Tab. S3); 11
372 have been investigated by immunoblotting approaches in previous studies. Heat maps visualize
373 the protein abundance of three independent experiments of mitochondria purified from leaves
374 and cell cultures. Proteins with high and low abundance are depicted in yellow and black,
375 respectively.

376

377 In addition, at least 16 outer envelope (OE)-localized proteins from plastids were co-purified
378 with mitochondria, with higher abundance in C-mito (Fig. 8). They account for 3.4 % (16/471) of
379 the identified plastidial proteins, which are enriched by more than two folds in comparison to
380 the proportion of OE proteins in plastids (46/3002, 1.5 %) (Inoue, 2007, 2011; Simm et al., 2013;
381 Kim et al., 2019). The enrichment of OE proteins in mitochondrial extracts suggests for a close
382 physical interaction between mitochondria and plastidial OE membrane. For instance, the
383 membrane contact sites, which were not disrupted during the isolation procedure, and
384 therefore are present in the mitochondrial samples as membrane patches.

L-mito	C-mito	Locus	Name	Function
		AT2G16640	TOC132	Translocon complex in the outer envelope membrane 132
		AT2G28900	OEP16-1	Outer plastid envelope protein 16-1
		AT2G43950	OEP37	Outer envelope protein 37
		AT3G06510	GGGT	Galactolipid:galactolipid galactosyltransferase
		AT3G17970	TOC64-III	Translocon at the outer membrane of chloroplasts 64-III
		AT3G46740	TOC75-III	Translocon at the outer envelope membrane of chloroplasts 75-III
		AT3G52420	OEP7	Outer envelope membrane protein 7
		AT4G02510	TOC159	Translocon at the outer envelope membrane of chloroplasts 159
		AT5G05000	TOC34	Translocon at the outer envelope membrane of chloroplasts 34
		AT5G19620	OEP80	Outer envelope protein of 80 kDa

385

386 **Figure 8.** Identified plastid outer envelope proteins in mitochondrial extracts. Our proteomic
387 analyses identified 12 outer envelope-localized proteins. Heat maps visualize the protein
388 abundance of three independent experiments of mitochondria purified from leaves and cell
389 cultures. Proteins with high and low abundance are depicted in yellow and black, respectively.

390

391

392 **Discussion**

393 In this study, we present an in-depth dataset of lipid molecular species from glycerolipids,
394 sphingolipids and sterols of Arabidopsis leaf mitochondria. With the assistance of online
395 resources, we assigned and confirmed central lipid biosynthesis steps within these
396 mitochondrial fractions. Furthermore, we confirmed and expanded our knowledge on the
397 existence of a protein complex for lipid trafficking between mitochondria and other organelles.
398 In the past, the most abundant plant mitochondrial glycerolipid classes, such as PC, PE, PI, PA,
399 CL, MGDG and DGDG, from *Arabidopsis* cell cultures and calli under phosphate-depleted
400 conditions have been quantified with TLC-GC (Michaud et al., 2017). However, a TLC-GC-based
401 approach lacks the molecular species information concerning acyl chain length and unsaturation
402 degree of the lipids, which are critical parameters to determine the membranes physical
403 properties. In addition, neither sphingolipids nor sterols of mitochondria were profiled to our
404 very best knowledge formerly in *Arabidopsis*.

405 In our study, mitochondria were purified by differential and Percoll density gradient
406 centrifugations. Much effort was made to document purity of the resulting organelle fraction: (i)
407 visual inspection of the protein complex composition by 2D BN / SDS PAGE and (ii) label-free
408 quantitative shotgun proteins in combination with SUBAcon evaluation. The SUBAcon database
409 integrates worldwide knowledge on subcellular localization information of Arabidopsis proteins
410 based on *in vitro* or *in vivo* protein targeting experiments, mass spectrometry-based analyses of
411 organellar fractions, protein-protein interaction data and bioinformatics tools for subcellular
412 localization prediction. Based on the latter approach, purity of our mitochondrial fractions can
413 be estimated to be in the range of 90% (87 to 94%, Supplemental Fig. S2). Traces of chloroplasts
414 were present in our fractions. However, even Rubisco, which is considered to be the most
415 abundant chloroplast protein, was detectable only as a very faint spot on the 2D BN/SDS gel of
416 the L-mito fraction (Fig. 1). Finally, quantitative lipidomics revealed the purity of our
417 mitochondrial fraction. MGDG, DGDG, PG and SQDG are the main components of plastidial
418 membranes (Hölzl and Dörmann, 2019). In *Arabidopsis* chloroplasts, the ratio of MGDG : DGDG :
419 PG : SQDG is about 1:0.5:0.1:0.3 (Awai et al., 2006). In contrast, a distinct ratio of 1:0.3:0.4:0 was
420 detected in L-mito in this study (Fig. 2). Moreover, only a few specific MGDG and DGDG
421 molecular species are enriched in L-mito compared to L-TE (Fig. 3B), suggesting that the cross-

422 contamination from intact plastids or bulk plastidial membranes are insignificant. On the other
423 hand, more than 85 % of the subunits of the MTL complex (deduced from its composition in
424 yeast mitochondria, Fig. 7) and many OE proteins (Fig. 8) were identified in the mitochondrial
425 samples via our proteomics approach, strongly suggesting that a close contact between
426 mitochondria, the ER and chloroplasts exists in our preparations. We conclude that the
427 identified chloroplast lipids and proteins rather originate from small pieces of plastidial
428 membranes and, importantly, the mitochondria-plastid contact sites, which are present in our
429 mitochondrial fraction and contribute to the measured lipid composition. While the protein
430 complexes connecting ER and mitochondria have been well described in yeast, their roles in
431 mediating and/or facilitating lipid translocation are less defined in plants. In contrast to yeast, to
432 our knowledge only one tethering protein has been described in flowering plants up to now
433 (Michaud et al., 2016).

434 With the proteomic and lipidomic datasets as well as the online resources in hand, we assigned
435 central lipid biosynthesis reactions and refined models for a possible exchange of lipid
436 molecules between mitochondria, ER and plastids in plants in Fig. 9. Previous studies in yeast
437 and mammalian cells have shown that mitochondria are capable of synthesizing PE, PA, PG and
438 CL (Flis and Daum, 2013; Horvath and Daum, 2013; Tatsuta et al., 2014). Here, we expand the
439 knowledge that at least the glycerolipids PE and CL can be generated and/or modified in
440 Arabidopsis leaf mitochondria. Considering PE biosynthesis, the rate-limiting enzymes in CDP-
441 ethanolamine and PS decarboxylation pathways, PECT1 and PSD1, respectively, were identified
442 in our mitochondrial samples with higher abundance in C-mito (Fig. 4). It suggests that the
443 generation of mitochondrial PE in the cell culture may be more active in comparison to the
444 leaves. Moreover our observation was supported by earlier studies that localized PECT1 at the
445 mitochondrial periphery and PSD1 in mitochondria in *Arabidopsis* (Mizoi et al., 2006; Nerlich et
446 al., 2007). PE is one of the most abundant glycerophospholipids in biological membranes.
447 Therefore, a high demand is expected to supply mitochondria for their biogenesis in actively
448 dividing cell cultures. The other major component of biological membranes is PC. It is
449 considered to be synthesized in the ER and then transferred through protein complexes
450 connecting ER and mitochondria to mitochondria. The structural information of the enriched
451 lipid species provides evidences for the biosynthesis in the ER as well. Many PE and PC species in

452 mitochondrial samples have longer acyl moieties with 22 to 26 carbons, which can only be
453 synthesized in the ER (Haslam and Kunst, 2013). Conventionally, the majority of PS biosynthesis
454 was assumed to take place in the ER and before being transferred to mitochondria as well. PS
455 and PE, although they are able to interconvert, have distinct lipid profiles from each other,
456 suggesting that only selected lipid species are the substrates of PSD1. In addition, inositol
457 polyphosphate phosphatase 1 (SAL1), which is an enzyme that is involved in phosphoinositide
458 degradation and generates inositol phosphates, was identified in our mitochondrial samples
459 with higher abundance in C-mito comparing to L-mito. This finding confirmed a previous report
460 that localized it in both mitochondria and plastids (Estavillo et al., 2011). Inositol phosphates
461 play crucial roles in many biological processes including gene expression and regulation of cell
462 death through sphingolipids (Alcázar-Román and Wente, 2008; Donahue et al., 2010). Removal
463 of head groups from glycerophospholipids, mostly PC and PE, by phospholipase Dα1 (PLDα1)
464 results in PA, serving as important precursor in other glycerophospholipid biosynthesis
465 pathways (Fig. 9). Comparing to L-TE, the most enriched PA species in L-mito carry 16:0 and 18:0
466 fatty acyl moieties. This corresponds to the enriched PI, PG and DAG species in L-mito,
467 suggesting that PA may serve as an interconverting hinge between these glycerolipids in plant
468 mitochondria. While our study detected PLDα1 preferentially in C-mito samples, previous
469 studies localized it in the cytosol or at the plasmamembrane (Du et al., 2013). This may suggest
470 that PLDα1 localizes to contact sites either between plasmamembrane and mitochondria or
471 between ER and mitochondria. In addition, two glycerol-3-phosphate dehydrogenases were
472 identified (SDP6 and GPDHp). Whereas SDP6 was detected in mitochondria before, GPDHp was
473 localized in the plastid (Nandi et al., 2004; Quettier et al., 2008).

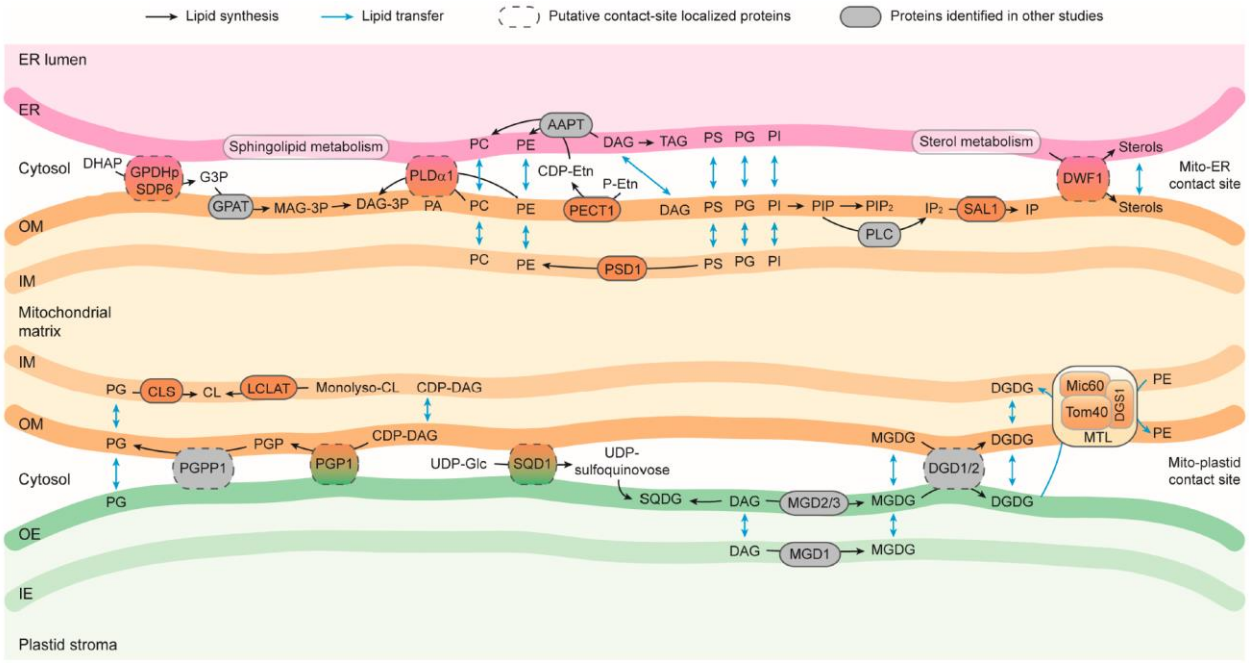

Figure 9. Model of lipid biosynthesis and trafficking within and between mitochondria, ER and plastids in *Arabidopsis*. Lipid synthesis and transfer between membranes are indicated by black and blue arrows, respectively. Proteins identified in L-mito or C-mito with additional ER or plastidic localization based on The Arabidopsis Information Resource (TAIR; www.arabidopsis.org) and the Subcellular localization database for Arabidopsis proteins (SUBAcon; www.suba.live) are considered as putative contact-site localized proteins (dashed frame). Lipid biosynthesis-related proteins indicated in other studies are depicted in grey. Full names and functions of involved proteins are itemized in Supplemental Tab. S1. OM, mitochondrial outer membrane; IM, mitochondrial inner membrane; OE, plastid outer envelope; IE, plastid inner envelope; MTL, mitochondrial transmembrane lipoprotein complex. DHAP, dihydroxyacetone phosphate; G3P, glyceraldehyde 3-phosphate; MAG, monoacylglycerol; DAG, diacylglycerol; Etn, ethanolamine; TAG, triacylglycerol; IP, inositol phosphate; PGP, phosphatidylglycerol phosphate; SQDG, sulfoquinovosyl diacylglycerol.

An enzyme being involved in synthesizing PG from PA is PGP1. It was found in our proteomic analysis in C-mito samples (Fig. 4). CL can be synthesized through condensation of PG and DAG by CLS, or addition of acyl chains to monolyso-CL by monolysocardiolipin acyltransferase (LCLAT or Tafazzin). All identified enzymes involving in PG and CL biosynthesis, PGP1, CLS and LCLAT,

493 are more abundant in C-mito compared to L-mito. PGP1 was previously found to localize to both
494 mitochondria and plastids (Babiychuk et al., 2003), while CLS was localized to mitochondria
495 (Katayama et al., 2004). This suggests an intensive interaction between mitochondria and
496 plastids in cell cultures because (1) high amounts of proteins localized in contact sites imply a
497 closer connection between the two organelles; (2) more CLS is required to convert the plastid-
498 derived PG which is transferred to mitochondria presumably via membrane contact sites; (3)
499 active energy generation is vital for actively dividing cells and thus a high amount of CL is
500 required to assemble the respiratory chain complexes in mitochondria. Although PG is the
501 precursor for CL synthesis, the abundance in L-mito is significantly less than in L-TE, probably
502 because a substantial amount in L-TE originates from plastids and PG is directly converted into
503 CL in mitochondria (Fig. 2).

504 Typically, glyceroglycolipids such as MGDG, DGDG and SQDG are considered to be synthesized in
505 plastids and are transferred to other organelles upon stress. For instance, DGDG is transferred
506 from plastidial membranes to other compartments including mitochondrial membranes and the
507 plasma membrane during phosphate starvation to compensate the loss of PC and PE (Jouhet et
508 al., 2004). In addition to vesicular transportation and lipid trafficking via contact sites, emerging
509 evidences support the hypothesis of lipid synthesis in *trans* in yeast and plants (Mehrshahi et al.,
510 2013; Tavassoli et al., 2013; Michaud et al., 2017). That is, enzyme located at one membrane
511 might be capable to catalyze the reaction on another membrane when they are in close
512 apposition. In this way, neither tethering proteins nor massive lipid remolding under stress
513 conditions is required, if the mitochondria can acquire lipids without setting up the junctions to
514 other organelles. Therefore, we suspect that the DGDG biosynthesis enzymes, DGD1/2, catalyze
515 the reactions in *trans* or at the mitochondria-plastid contact sites, providing DGDG molecules to
516 compensate the loss of glycerophospholipids in real time (Fig. 4b). In addition, several subunits
517 of the MTL complex were identified in our proteomic approach including Tom40, Mic60, DGS1
518 etc. (Fig. 7). It establishes a lipid trafficking system removing DGDG from plastids and allocating
519 PE between the IM and OM. Rapid remodeling of the mitochondrial membranes is supported by
520 in *trans* lipid biosynthesis and the MTL complex, likely in close cooperation with other
521 complexes. However, the underlying mechanism of this lipid transportation machinery is still
522 largely unknown. SQDG synthase (SQD1) was identified exclusively in C-mito, but no SQDG

523 molecules were detected (Fig. 4b). Earlier reports localized SQD1 in chloroplasts (Essigmann et
524 al., 1998), suggesting that SQD1 is either co-purified with plastid envelope membranes from cell
525 cultures or is localized in .

526 Sphingolipid biosynthesis takes place at the ER membrane and subsequently in the Golgi
527 apparatus for the addition of carbohydrate residues. Interestingly, in the last decade, several
528 sphingolipid-metabolizing enzymes have been identified in mitochondria purified from yeast
529 and mammalian systems, including Cer synthase and ceramidase (Bionda et al., 2004; Kitagaki et
530 al., 2007; Novgorodov et al., 2011). In animal models, mitochondria-synthesized Cer plays a
531 crucial role in cerebral ischemia-induced mitochondrial dysfunction. The connection between
532 sphingolipids and mitochondria-promoted apoptosis has been proposed in plants as well.
533 Recent studies in *Arabidopsis* have demonstrated that the ratio between LCB-P and Cer is
534 involved in maintaining the balance of cell survival and apoptosis (Watanabe et al., 2013; Bi et
535 al., 2014). However, no sphingolipid biosynthesis enzyme has been identified in plant
536 mitochondria hereto. GIPCs are the most abundant sphingolipids in mitochondria, although still
537 minor comparing to glycerophospholipids. It is known that PM-localized GIPCs are important in
538 signal transduction and intercellular recognition (Lenarčič et al., 2017; Ali et al., 2018). GIPCs
539 may as well establish the communication between mitochondria and other organelles, although
540 further analysis is required to understand the functions of sphingolipids in plant mitochondria.

541 Sterols, although taking part in both biotic and abiotic stress responses, are at low abundance in
542 mitochondrial samples. Sterol biosynthesis primarily takes place in the ER (Schaller, 2003).
543 Among them, sterol C-24 reductase (DWF1) was identified both in L-mito and C-mito, with
544 higher abundance in C-mito. DWF1 has been proposed to mediate the biosynthesis of all
545 phytosterols with higher specificity towards campesterol in Arabidopsis, but this protein was
546 localized to ER membranes (Klahre et al., 1998; Youn et al., 2018). Therefore, we suggest DWF1
547 as an additional contact site localized protein (Fig. 7). High amount of campesterol was detected
548 in L-mito, suggesting the existence of an onsite biosynthesis and/or sterol transporter to
549 facilitate the import of campesterol from the ER. However, unlike mammalian cells wherein
550 cholesterol transport proteins such as steroidogenic acute regulatory protein, StAR (Clark et al.,
551 1995), and MLN64 (Charman et al., 2010) have been identified, little is known about sterol
552 transporters in plants.

553 **Conclusions**

554 In summary, we expanded the knowledge regarding lipid biosynthesis and modification in plant
555 mitochondria by performing a global lipidome analysis of Arabidopsis leaf mitochondria to
556 provide their in-depth lipid molecular species profile including glycerolipids, sphingolipids and
557 sterols. Our proteome data confirmed that PE and CL can be synthesized in these organelles
558 partially by the assistance of putative contact-site localized proteins and / or in *trans* lipid
559 biosynthesis. Based on the proteomic results, we propose and confirm the existence of
560 membrane contact site-localized proteins and their aspects in lipid biosynthesis pathways. This
561 study serves as a foundation for additional researches in unveiling the functional roles of
562 mitochondrial lipids and the mechanisms of mitochondria-dependent signaling pathways.

563

564 **Materials and methods**

565 **Plant materials and growth conditions**

566 Rosette leaves of wild-type *Arabidopsis thaliana* (L.) Heynh Columbia-0 were used for both
567 extracting total lipid extract and purifying mitochondria. After sowing the seeds in pots with
568 three-day cold stratification at 4 °C, seedlings were grown under 16 h-day length at 24 °C with
569 60 % relative humidity and 150 µmol photons m^{-2} sec^{-1} for one week. Young seedlings were
570 transferred to large trays and grown with equal spacing for another three weeks before further
571 experimental procedures.

572 **Suspension culture of *Arabidopsis thaliana***

573 Suspension cultures were established starting from sterilized seeds of *Arabidopsis thaliana* wild-
574 type Columbia-0, grown on MS medium plates containing 0.8 % agar. Plant pieces were
575 transferred to B5 medium agar plates and cultivated for several weeks in the dark for callus
576 induction. Callus was finally transferred into liquid B5 medium including 3 % (w/v) sucrose,
577 0.01 % (w/v) 2,4-dichlorophenoxyacetic acid and 0.001 % (w/v) kinetin. Cultures were incubated
578 on a shaker at 24 °C in the dark. Callus was transferred weekly into new liquid medium (3 g /
579 100 ml).

580 **Mitochondria isolation**

581 *From Arabidopsis rosettes*

582 The mitochondria isolation procedure was described previously (Schikowsky et al., 2018). About
583 200 g of four-week-old *Arabidopsis* rosettes were collected and homogenized at 4 °C with a
584 waring blender in 1 liter disruption buffer (0.3 M sucrose, 60 mM TES, 25 mM tetrasodium
585 pyrophosphate, 10 mM potassium dihydrogen phosphate, 2 mM EDTA, 1 mM glycine, 1 %
586 PVP40, 1 % BSA, 50 mM sodium ascorbate, 20 mM cysteine; pH 8.0) by three times for 10 sec
587 with 30 sec intervals. The following procedures were performed on ice or at 4 °C. Two layers of
588 miracloth with supporting gauze were used to filter the homogenate into a beaker. The
589 remaining plant debris was first grinded with additional sea sand for 10 min by mortar and
590 pestle, and then filtered again through miracloth. The filtrates were combined and centrifuged
591 at 2,500 g for 5 min to eliminate the cell debris. Centrifugation with higher speed at 15,250 g for
592 15 min was applied on the supernatant to pellet mitochondria and other organelles. The
593 resulting pellets were resuspended with a paintbrush in wash buffer (0.3 M sucrose, 10 mM TES,
594 10 mM potassium dihydrogen phosphate; pH 7.5). The samples were adjusted to the final
595 volume of 12 ml with wash buffer and transferred to a Dounce homogenizer. Two strokes of
596 pestle were performed to disrupt large organelles like chloroplasts. Aliquots of 1 ml samples
597 were transferred carefully to Percoll gradients which had been established beforehand by
598 69,400 g centrifugation for 40 min in one-to-one ratio of Percoll and Percoll medium (0.6 M
599 sucrose, 20 mM TES, 2 mM EDTA, 20 mM potassium dihydrogen phosphate, 2 mM glycine;
600 pH 7.5). Mitochondria were separated from other components by centrifuging in the gradients
601 at 17,400 g for 20 min. The resulting mitochondrial fractions formed white clouds at the bottom
602 half of the gradients and were collected by Pasteur pipettes to clean centrifuge tubes. The
603 clean-up procedures were performed three to five times by filling up wash buffer in the
604 centrifuge tubes and pelleting the mitochondria with 17,200 g for 20 min, until the resulting
605 pellet was firm. After each washing steps, two to three pellets were combined in one tube until
606 all mitochondria from one biological replicate were pooled together. The mitochondrial pellets
607 were weighed, resuspended with wash buffer and aliquoted at the concentration of 0.1 g/ml.

608 *From cell cultures*

609 Mitochondria isolation from *Arabidopsis thaliana* suspension cell culture was carried out as
610 described before (Farhat et al., 2019). About 200 g fresh cells were harvested and homogenized
611 using disruption buffer (450 mM sucrose, 15 mM MOPS, 1.5 mM EGTA, 0.6 % (w/v) PVP40, 2 %
612 (w/v) BSA, 10 mM sodium ascorbate, 10 mM cysteine; pH 7.4) and a waring blender. During
613 several washing steps, cell fragments were removed (centrifugation twice for 5 minutes at
614 2,700 g and once for 5 minutes at 8,300 g). Crude mitochondria were pelleted at 17,000 g for
615 10 minutes, resuspended in washing buffer (0.3 M sucrose, 10 mM MOPS, 1 mM EGTA; pH 7.2),
616 homogenized using a Dounce homogenisator and loaded onto discontinuous Percoll gradients
617 (phases of 18 %, 23 % and 40 % Percoll in gradient buffer (0.3 M sucrose, 10 mM MOPS, 0.2 mM
618 EGTA; pH 7.2)). After ultracentrifugation (90 minutes, 70,000 g), purified mitochondria were
619 collected from the 23 %-40 % interphase. For Percoll removal, several washing steps
620 (10 minutes, 14,500 g) were performed using resuspension buffer (0.4 M mannitol, 1 mM EGTA,
621 10 mM tricine; pH 7.2) to gain a firm pellet of purified mitochondria.

622 Each of the three independently purified mitochondria populations from 4-week old rosette
623 leaves (L-mito) and 200 g cell cultures (C-mito), respectively were used for all experiments.

624 **BN/SDS-PAGE**

625 Gel electrophoresis procedures (blue-native (BN) and SDS PAGE) were performed as described
626 previously (Senkler et al., 2018), based on the published protocol given in (Wittig et al., 2006).

627 **Label-free quantitative shotgun proteomics**

628 *Protein sample preparation*

629 Sample preparation for shotgun proteome analysis was performed as described before (Thal et
630 al., 2018). The protein content of the mitochondrial fractions was determined using a Bradford
631 assay kit (Thermo Scientific, Rockford, USA). 50 µg protein of each sample were loaded onto a
632 SDS gel for sample purification (Thal et al., 2018). Electrophoresis was stopped when the
633 proteins reached the border between the stacking and the separating gel. Gels were
634 subsequently incubated in fixation solution (15% (v.v) ethanol; 10% (v.v) acetic acid) for 30 min,
635 stained for 1 h with Coomassie Brilliant Blue G250, and finally the protein band at the border of

636 the two gel phases was cut out into cubes with edge lengths of approximately 1 mm.
637 Trypsination of the proteins was carried out as described previously (Fromm et al., 2016).

638 *Shotgun proteomic LC-MS analysis*

639 Label-free quantitative mass spectrometric analyses of whole mitochondrial protein samples
640 from cell culture and long day *Arabidopsis thaliana* leaves were performed as outlined before
641 (Thal et al., 2018) using an Ultimate 3000 UPLC coupled to a Q Exactive Orbitrap mass
642 spectrometer (Thermo Scientific, Dreieich, Germany).

643 *Data processing*

644 In a first step, the resulting MS data were processed using the Proteome Discoverer Software
645 (Thermo Fisher Scientific, Dreieich, Germany) and searched with the Mascot search engine
646 (www.matrixscience.com) against the tair10 protein database (downloaded from
647 www.arabidopsis.org). For quantitative analyses, MS data were further processed as outlined
648 before (Rugen et al., 2019) using the MaxQuant software package (version 1.6.4.0), the
649 Andromeda search engine (Cox and Mann, 2008) and the tair10 protein database. For
650 determination of sample purity, peptide intensities were used, combined with the subcellular
651 locations of assigned proteins as given by SUBAcon from the SUBA platform (www.suba.live)
652 (Hooper et al., 2017). A proteomic heatmap was generated using the NOVA software
653 (www.bioinformatik.uni-frankfurt.de/tools/nova/index.php)(Giese et al., 2015). Identified
654 proteins of all six datasets (three biological replicates of leave total mitochondrial protein (L-
655 mito 1,2,3) and cell culture total mitochondrial protein (C-mito 1,2,3)) were hierarchically
656 clustered in a heatmap based on iBAQ (intensity Based Absolute Quantification) values (for
657 primary results see Supplemental Tab. S1).

658 **Lipid extraction**

659 Total lipid extract from leaf (L-TE) was obtained as described (Tarazona et al., 2015). Briefly,
660 mixture of 150 mg frozen leaf powder or 100 mg mitochondria and 6 ml extraction buffer
661 (propan-2-ol : hexane : water, 60:26:14 (v.v.v)) was incubated at 60 °C with shaking for 30 min.
662 After centrifugation at 800 g for 20 min, the clear supernatant was transferred to clean tubes
663 and evaporated under stream of nitrogen gas until dryness. Samples were reconstituted in

664 800 µl of TMW (tetrahydrofuran (THF) : methanol : water, 4:4:1 (v.v.v)). Procedure for extracting
665 the mitochondrial lipids was adjusted by substituting the water fraction of the extraction buffer
666 by equal volume of the mitochondrial aliquot. Further process was continued as described
667 above.

668 **TLC-GC quantification**

669 *TLC separation of lipid classes*

670 Lipid extracts from 500 mg mitochondria and 50 mg leaves were spotted onto TLC 60 plates (20
671 × 20 cm^2, Merck KGaA, Darmstadt, Germany) in parallel with corresponding standards (Merck
672 KGaA). Extracts were developed by a solvent mixture of chloroform : methanol : acetic acid
673 (65:25:8 (v.v.v)). After visualizing the lipid spots under 528 nm UV light, the bands were
674 scrapped out and converted to fatty acid methyl esters (FAME) before GC analysis.

675 *Acidic transesterification*

676 Glycerolipids were transesterified by acidic methanolysis (Miquel and Browse, 1992) and
677 converted to fatty acid methyl esters (FAME). The lipid-bound silica powder from corresponding
678 spots on TLC plate were scrapped out and added to 1 ml FAME solution (methanol : toluene :
679 sulfuric acid : dimethoxypropane, 33:17:1.4:1 (v.v.v.v)) with 5 µg tripentadecanoin as an internal
680 standard. After 1 h incubation at 80 °C, 1.5 ml saturated NaCl solution and 1.2 ml hexane were
681 added subsequently. The resulting FAME was collected from the hexane phase, dried, and
682 reconstituted in 10 µl acetonitrile.

683 *GC/FID analysis*

684 Lipid-bound fatty acids were analyzed after converting to FAMEs by a 6890N Network GC/FID
685 System with a medium polar cyanopropyl DB-23 column (30 m × 250 µm × 25 nm; Agilent
686 Technologies, Waldbronn, Germany) using helium as the carrier gas at 1 ml min^{-1}. Samples were
687 injected at 220 °C with an Agilent 7683 Series injector in split mode. After 1 min at 150 °C, the
688 oven temperature raised to 200 °C at the rate of 8 °C min^{-1}, increased to 250 °C in 2 min, and
689 held at 250 °C for 6 min. Peak integration was performed using the GC ChemStation (Agilent
690 Technologies).

691 **Lipid derivatization**

692 Phosphate-containing lipids - phosphatidic acids (PA), phosphoinositides (PIPs) and long-chain
693 base phosphates (LCB-P) - were derivatized to enhance their chromatographic separation and
694 mass spectrometric detection. Methylation procedure was applied on PA and PIPs as followed.
695 Aliquots of 100 µl lipid extracts were first brought to dryness under stream of nitrogen gas and
696 reconstituted with 200 µl methanol. Methylation reaction took place after the supply of 3.3 µl
697 trimethylsilyldiazomethane. After 30 min incubation at room temperature, the reaction was
698 terminated by neutralizing with 1 µl of 1.7 M acetic acid. Samples were dried under nitrogen gas
699 and redissolved in 100 µl TMW. Acetylation procedure was applied on LCB-P. Aliquots of 100 µl
700 lipid extracts were brought to dryness and reconstituted with 100 µl pyridine and 50 µl acetic
701 anhydride. After 30 min incubation at 50 °C, samples were dried under stream of nitrogen gas
702 with 50 °C water bath. To redissolve the samples, 100 µl TMW was used as the final solvent to
703 proceed with lipid analysis.

704 **Global lipidomic analysis with LC-MS**

705 Analysis conditions and system setup were as described (Tarazona et al., 2015). Samples were
706 separated by an ACQUITY UPLC system (Waters Crop., Milford, MA, USA) with a HSS T3 column
707 (100 mm x 1 mm, 1.8 µl; Waters Crop.), ionized by a chip-based nanoelectrospray using TriVersa
708 Nanomate (Advion BioScience, Ithaca, NY, USA) and analyzed by a 6500 QTRAP tandem mass
709 spectrometer (AB Sciex, Framingham, MA, USA). Aliquots of 2 µl were injected and separated
710 with a flow rate of 0.1 ml min^{-1}. The solvent system composed of methanol : 20 mM ammonium
711 acetate (3:7 (v.v)) with 0.1 % (v.v) acetic acid (solvent A) and THF : methanol : 20 mM
712 ammonium acetate (6:3:1 (v.v.v)) with 0.1 % (v.v) acetic acid (solvent B). According to the lipid
713 classes, different linear gradients were applied: start from 40 %, 65 %, 80 % or 90 % B for 2 min;
714 increase to 100 % B in 8 min; hold for 2 min and re-equilibrate to the initial conditions in 4 min.
715 Starting condition of 40 % solvent B were utilized for long-chain bases (LCB) and phosphorylated
716 long-chain bases (LCB-P); 80 % for diacylglycerol (DAG); 90 % for steryl esters (SE); 65 % for the
717 remaining lipid classes. Retention time alignment and peak integration were performed with
718 MultiQuant (AB Sciex). Quantitative results were calculated according to the amount of internal
719 standards.

720 **Biosynthesis pathways construction**

721 The Arabidopsis Information Resource (TAIR; www.arabidopsis.org), the Subcellular localization
722 database for Arabidopsis proteins (SUBAcon; www.suba.live), Kyoto Encyclopedia of Genes and
723 Genomes (KEGG; www.genome.jp/kegg) and the shotgun proteomic analyses of L-mito and C-
724 mito were combined to construct the lipid biosynthesis pathways in plant mitochondria.
725 Additionally, lipidomics data are depicted in the pathways to illustrate the biosynthetic fluxes.

726

727 **Supplemental Data**

728 **Supplemental Figure S1.** Purity inspection of mitochondrial protein complexes and
729 supercomplexes by two-dimensional blue-native/SDS PAGE. Mitochondrial fractions isolated
730 from Arabidopsis leaves (L-mito 1 and L-mito 3) and from Arabidopsis cell cultures (C-mito1 and
731 C-mito 3) were separated by 2D PAGE and Coomassie-stained (corresponding gels of fractions L-
732 mito 2 and C-mito 2 see Fig. 1). Numbers on top and to the left of the 2D gels refer to the
733 masses of standard protein complexes / proteins (in kDa), the roman numbers above the gels to
734 the identity of OXPHOS complexes (see Fig. 1 for detailed information). The arrows indicate the
735 large (L; 53,5 kDa) and the small (S; 14.5 kDa) subunit of Rubisco. 2D blue-native/SDS reference
736 gels for mitochondrial and chloroplast fractions (Mito-ref, Cp-ref) from Arabidopsis thaliana are
737 given to the bottom of the figure (gels were taken from Klodmann et al. 2011 and Behrens et al.
738 2013). Identity of the protein complexes visible on the chloroplast reference gel: PSI –
739 photosystem I; PSII – photosystem II; Rub – Rubisco; LHCII – light harvesting complex II.

740 **Supplemental Figure S2.** Purity of mitochondrial fractions as determined by label-free quantitative
741 shot gun proteomics. Three mitochondrial fractions isolated from Arabidopsis leaves (L-mitos) and cell
742 cultures (C-mitos) were analysed. Summed-up peptide intensities were calculated for subcellular
743 compartments based on protein assignments as given by SUBAcon (The Subcellular localization database
744 for Arabidopsis proteins; www.suba.live**).** Blue: mitochondria; green: plastids; gray: others; numbers in
745 %.

746 **Supplemental Figure S3.** Fatty acid profiles of the glycerolipids from L-mito, L-TE, C-mito and C-TE.
747 Heat maps illustrate the difference of the fatty acid distribution based on LC-MS/MS analyses. Each

748 column represents one lipid class wherein the acyl moieties of all species are listed and summarized to
749 100 %. Data represent mean values in mol % from three independent experiments.

750 **Supplemental Figure S4.** Workflow for the construction of the biosynthesis pathways. Multiple
751 databases were combined to build the lipid biosynthesis pathways in mitochondria, The Arabidopsis
752 Information Resource (TAIR; www.arabidopsis.org), the Subcellular localization database for Arabidopsis
753 proteins (SUBAcon; www.suba.live), Kyoto Encyclopedia of Genes and Genomes (KEGG;
754 www.genome.jp/kegg) and the proteomic datasets of isolated mitochondria in this study. Information of
755 protein localizations and backbones of the biosynthesis pathways were obtained from TAIR, SUBAcon
756 and KEGG, respectively.

757 **Supplemental Figure S5.** Additional lipid biosynthesis enzymes which do not match with analyzed lipid
758 classes in this study. Enzymes of (a) fatty acid biosynthesis, (b) unsaturated fatty acid biosynthesis, (c)
759 lipoic acid metabolism and (d) ubiquinone and other terpenoid-quinone biosynthesis illustrate the
760 general lipid biosynthesis in Arabidopsis mitochondria. Heat maps visualize the protein abundance based
761 on shotgun proteomic analyses of three independent experiments of purified mitochondria from leaves
762 and cell culture. Blue: proteins identified in the proteomic analysis of this study and also predicted to
763 localize in mitochondria; green: proteins identified in the proteomic analysis of this study but predicted
764 to localize in other organelles; bold font: exclusively localized in mitochondria; italic font: only identified
765 in one of the mitochondrial populations. Further full names and functions are itemized in Table S1. In the
766 heat maps, proteins with high and low abundance are depicted in yellow and black, respectively.
767 Predicted protein localization was based on The Arabidopsis Information Resource (TAIR;
768 www.arabidopsis.org) and the Subcellular localization database for Arabidopsis proteins (SUBAcon;
769 www.suba.live).

770 **Supplemental Table S1.** Overall proteins identified in the proteomic approach.

771 **Supplemental Table S2.** Overall lipids identified in the lipidomic approach.

772 **Supplemental Table S3.** Lipid biosynthesis-related proteins identified in the proteomic
773 approach.

774

775

776

Acknowledgements

We are grateful for the technical assistance from Sabine Freitag. YL has been a doctoral student of the Ph.D. program "Molecular Biology" – International Max Planck Research School and the Göttingen Graduate School for Neurosciences, Biophysics, and Molecular Biosciences (GGNB) (DFG grant GSC 226) at the Georg August University Göttingen.

Funding information

IF and HPB acknowledge funding through the German Research Foundation (DFG: INST 186/822-1, INST 186/1167-1, INST 187/503-1 and ZUK 45/2010).

Figure legends

Figure 1. Purity of mitochondrial fractions. The purity of mitochondrial fractions was determined by 2D blue native / SDS PAGE **(A)** and by summed-up peptide intensities of subcellular compartments based on protein assignments as given by the Subcellular localization database for Arabidopsis proteins (SUBAcon; www.suba.live) **(B).**

A: Mitochondria were isolated from *Arabidopsis* leaves (L-mito) and cell cultures (C-mito). Proteins were separated by 2D Blue native PAGE and Coommassie-stained. Numbers on top and to the left of the 2D gels refer to the masses of standard protein complexes / proteins (in kDa), the roman numbers above the gels to the identity of OXPHOS complexes. I+III_2: supercomplex consisting of complex I and dimeric complex III; I: complex I; V: complex V; III_2: dimeric complex III; IV: complex IV. The small (S; 14.5 kDa) and the large (L; 53.5 kDa) subunit of Rubisco are indicated by green arrows. Biological replicates of the 2D gels and reference gels for mitochondrial and chloroplast fractions from *Arabidopsis* are shown in Fig. S1.

B: Mitochondrial fractions from *Arabidopsis* leaves and cell cultures were analyzed by label-free quantitative shotgun proteomics. Peptide intensities assigned to subcellular compartments were summed-up and averaged results for L-mitos and C-mitos were visualized by pie charts (for detailed results see Fig. S2). Blue: mitochondria; green: plastids; gray: others; numbers in %.

804 **Figure 2.** Lipid class profiles of purified mitochondria and total leaf extracts. Glycerolipids of leaf
805 total extract (L-TE) and mitochondria isolated from leaves (L-mito) were analyzed quantitatively
806 by TLC-GC approach. Data of L-TE represent mean values in mol % from three independent
807 experiments ± SD; data of L-mito represent mean values in mol % from two independent
808 experiments ± SEM. PC, phosphatidylcholine; PE, phosphatidylethanolamine; CL, cardiolipin; PG,
809 phosphatidylglycerol; MGDG, monogalactosyldiacylglycerol; DGDG, digalactosyldiacylglycerol.

810

811 **Figure 3.** Profiles of molecular glycerolipid species and the according fold changes between L-
812 mito and L-TE. Heat maps of (a) glycerophospholipids, (b) glyceroglycolipids and (c)
813 diacylglycerols illustrate the difference of species distribution based on LC-MS/MS analyses.
814 Each block represents one lipid class wherein the detected species are presented and
815 summarized to 100 %. Data represent mean values in mol % from three independent
816 experiments. Binary logarithm was applied when the mean values are higher than 0.5 to inspect
817 the fold changes (FC) between L-mito and L-TE. One and two asterisks (*, **) indicate p values <
818 0.05 and < 0.01, respectively, by Student's t-test. PC, phosphatidylcholine; PE,
819 phosphatidylethanolamine; PS: phosphatidylserine; PI: phosphatidylinositol; PA phosphatidic
820 acid; DAG: Diacylglycerol; CL, cardiolipin; PG, phosphatidylglycerol; MGDG,
821 monogalactosyldiacylglycerol; DGDG, digalactosyldiacylglycerol.

822

823 **Figure 4.** Mitochondrial localized proteins that are related to glycerolipid biosynthesis. (a)
824 Glycerophospholipid, (b) glyceroglycolipid and (c) phosphoinositide metabolism. Proteins
825 identified and/or localized in mitochondria were labeled (i) blue: proteins identified in the
826 proteomic analysis of this study and also predicted to localize in mitochondria, (ii) green:
827 proteins identified in the proteomic analysis of this study in mitochondria but predicted to
828 localize in other organelles, (iii) bold font: exclusively localized in mitochondria and (iv) italic
829 font: only identified in one of the mitochondrial populations. Heat maps visualize the protein
830 abundance of three independent experiments of mitochondria purified from leaves and cell
831 cultures. Predicted protein localization was based on The Arabidopsis Information Resource

832 (TAIR; www.arabidopsis.org) and the Subcellular localization database for Arabidopsis proteins
833 (SUBAcon; www.suba.live).

834

835 **Figure 5.** Profiles of molecular sphingolipid species, the according fold changes between L-mito
836 and L-TE and general sphingolipid biosynthesis pathway in combination with mitochondrial
837 enriched lipids. Heat maps of (a) long chain bases, long chain base-phosphates and (b) complex
838 sphingolipids illustrate the difference of species distribution based on LC-MS/MS analyses. Each
839 block represents one lipid class wherein the detected species are presented and summarized to
840 100 %. Data represent mean values in mol % from three independent experiments. Binary
841 logarithm was applied when the mean values are higher than 0.5 to inspect the fold changes
842 (FC) between L-mito and L-TE. One and two asterisks (*, **) indicate p values < 0.05 and < 0.01,
843 respectively, by Student's t-test.

844

845 **Figure 6.** Profiles of molecular sterol species, the according fold changes between L-mito and L-
846 TE and general sterol biosynthesis pathway in combination of mitochondrial localized proteins
847 and enriched lipids. Heat maps of (a) free sterols (b) steryl glycosides (SG) and (c) acylated steryl
848 glycosides (ASG) and steryl esters (SE) illustrate the difference of species distribution based on
849 LC-MS/MS analyses. Each block represents one lipid class wherein the detected species are
850 presented and summarized to 100 %. Data represent mean values in mol % from three
851 independent experiments. Binary logarithm was applied when the mean values are higher than
852 0.5 to inspect the fold changes (FC) between L-mito and L-TE. One and two asterisks (*, **)
853 indicate p values < 0.05 and < 0.01, respectively, by Student's t-test.

854

855 **Figure 7.** MTL complex-associated proteins in mitochondria. Our proteomic analyses covered
856 186 of the 214 hypothetical subunits in the MTL complex (listed in Supplemental Tab. S3); 11
857 have been investigated by immunoblotting approaches in previous studies. Heat maps visualize
858 the protein abundance of three independent experiments of mitochondria purified from leaves

859 and cell cultures. Proteins with high and low abundance are depicted in yellow and black,
860 respectively.

861

862 **Figure 8.** Identified plastid outer envelope proteins in mitochondrial extracts. Our proteomic
863 analyses identified 12 outer envelope-localized proteins. Heat maps visualize the protein
864 abundance of three independent experiments of mitochondria purified from leaves and cell
865 cultures. Proteins with high and low abundance are depicted in yellow and black, respectively.

866

867 **Figure 9.** Model of lipid biosynthesis and trafficking within and between mitochondria, ER and
868 plastids in *Arabidopsis*. Lipid synthesis and transfer between membranes are indicated by black
869 and blue arrows, respectively. Proteins identified in L-mito or C-mito with additional ER or
870 plastidic localization based on The Arabidopsis Information Resource (TAIR;
871 www.arabidopsis.org) and the Subcellular localization database for Arabidopsis proteins
872 (SUBAcon; www.suba.live) are considered as putative contact-site localized proteins (dashed
873 frame). Lipid biosynthesis-related proteins indicated in other studies are depicted in grey. Full
874 names and functions of involved proteins are itemized in Supplemental Tab. S1. OM,
875 mitochondrial outer membrane; IM, mitochondrial inner membrane; OE, plastid outer envelope;
876 IE, plastid inner envelope; MTL, mitochondrial transmembrane lipoprotein complex. DHAP,
877 dihydroxyacetone phosphate; G3P, glyceraldehyde 3-phosphate; MAG, monoacylglycerol; DAG,
878 diacylglycerol; Etn, ethanolamine; TAG, triacylglycerol; IP, inositol phosphate; PGP,
879 phosphatidylglycerol phosphate; SQDG, sulfoquinovosyl diacylglycerol.

880

881 **References**

882 **Achleitner G, Gaigg B, Krasser A, Kainersdorfer E, Kohlwein SD, Perktold A, Zellnig G, Daum G** (1999)
883 Association between the endoplasmic reticulum and mitochondria of yeast facilitates
884 interorganelle transport of phospholipids through membrane contact. European Journal of
885 Biochemistry **264:** 545-553

886 **Alcázar-Román AR, Wente SR** (2008) Inositol polyphosphates: a new frontier for regulating gene
887 expression. Chromosoma **117:** 1-13
888 **Ali U, Li H, Wang X, Guo L** (2018) Emerging roles of sphingolipid signaling in plant response to biotic and
889 abiotic stresses. Mol Plant **11:** 1328-1343
890 **Awai K, Xu C, Tamot B, Benning C** (2006) A phosphatidic acid-binding protein of the chloroplast inner
891 envelope membrane involved in lipid trafficking. Proc Natl Acad Sci USA **103:** 10817-10822
892 **Babiychuk E, Müller F, Eubel H, Braun H-P, Frentzen M, Kushnir S** (2003) *Arabidopsis*
893 phosphatidylglycerophosphate synthase 1 is essential for chloroplast differentiation, but is
894 dispensable for mitochondrial function. Plant J **33:** 899 - 909
895 **Bi F-C, Liu Z, Wu J-X, Liang H, Xi X-L, Fang C, Sun T-J, Yin J, Dai G-Y, Rong C, Greenberg JT, Su W-W, Yao**
896 **N** (2014) Loss of ceramide kinase in *Arabidopsis* impairs defenses and promotes ceramide
897 accumulation and mitochondrial H_2O_2 bursts. Plant Cell **26:** 3449-3467
898 **Bionda C, Portoukalian J, Schmitt D, Rodriguez-Lafrasse C, Ardail D** (2004) Subcellular
899 compartmentalization of ceramide metabolism: MAM (mitochondria-associated membrane)
900 and/or mitochondria? Biochem J **382:** 527-533
901 **Birner R, Burgermeister M, Schneiter R, Daum G** (2001) Roles of phosphatidylethanolamine and of its
902 several biosynthetic pathways in *Saccharomyces cerevisiae*. Molecular Biology of the Cell **12:**
903 997-1007.
904 **Bligny R, Douce R** (1980) A precise localization of cardiolipin in plant cells. Biochim Biophys Acta **617:**
905 254-263
906 **Braun H-P** (2020) The Oxidative phosphorylation system of the mitochondria in plants. Mitochondrion
907 **53:** 66-75
908 **Cacas J-L, Furt F, Le Guédard M, Schmitter J-M, Buré C, Gerbeau-Pissot P, Moreau P, Bessoule J-J,**
909 **Simon-Plas F, Mongrand S** (2012) Lipids of plant membrane rafts. Prog Lipid Res **51:** 272-299
910 **Charman M, Kennedy BE, Osborne N, Karten B** (2010) MLN64 mediates egress of cholesterol from
911 endosomes to mitochondria in the absence of functional Niemann-Pick Type C1 protein. J Lipid
912 Res **51:** 1023-1034
913 **Clark BJ, Pezzi V, Stocco DM, Rainey WE** (1995) The steroidogenic acute regulatory protein is induced by
914 angiotensin II and K^+ in H295R adrenocortical cells. Molecular and Cellular Endocrinology **115:**
915 215-219
916 **Cox J, Mann M** (2008) MaxQuant enables high peptide identification rates, individualized p.p.b.-range
917 mass accuracies and proteome-wide protein quantification. Nature Biotechnol **26:** 1367-1372
918 **Daum G, Vance JE** (1997) Import of lipids into mitochondria. Prog Lipid Res **36:** 103-130

919 **Donahue JL, Alford SR, Torabinejad J, Kerwin RE, Nourbakhsh A, Ray WK, Hernick M, Huang X, Lyons**
920 **BM, Hein PP, Gillaspy GE** (2010) The *Arabidopsis thaliana myo*-inositol 1-phosphate synthase1
921 gene is required for *myo*-inositol synthesis and suppression of cell death. Plant Cell **22:** 888-903
922 **Douce R, Mannella CA, Bonner WD** (1972) Site of the biosynthesis of CDP-diglyceride in plant
923 mitochondria. Biochem Biophys Res Commun **49:** 1504-1509
924 **Du Z-Y, Chen M-X, Chen Q-F, Xiao S, Chye M-L** (2013) Arabidopsis acyl-CoA-binding protein ACBP1
925 participates in the regulation of seed germination and seedling development. Plant J **74:** 294-309
926 **Essigmann B, Guler S, Narang RA, Linke D, Benning C** (1998) Phosphate availability affects the thylakoid
927 lipid composition and the expression of *SQD1*, a gene required for sulfolipid biosynthesis in
928 *Arabidopsis thaliana*. Proc Natl Acad Sci USA **95:** 1950-1955
929 **Estavillo GM, Crisp PA, Pornsiriwong W, Wirtz M, Collinge D, Carrie C, Giraud E, Whelan J, David P,**
930 **Javot H, Brearley C, Hell R, Marin E, Pogson BJ** (2011) Evidence for a SAL1-PAP chloroplast
931 retrograde pathway that functions in drought and high light signaling in *Arabidopsis* Plant Cell
932 **23:** 3992-4012
933 **Farhat N, Hichri S, Hildebrandt TM, Debez A, Braun H-P** (2019) Composition and stability of the oxidative
934 phosphorylation system in the halophile plant *Cakile Maritima*. Front Plant Sci **10:** 1010
935 **Flis VV, Daum G** (2013) Lipid transport between the endoplasmic reticulum and mitochondria. Cold
936 Spring Harbor Perspectives in Biology **5:** a013235
937 **Fromm S, Senkler J, Eubel H, Peterhänsel C, Braun H-P** (2016) Life without complex I: proteome analyses
938 of an Arabidopsis mutant lacking the mitochondrial NADH dehydrogenase complex. J Exp Bot **67:**
939 3079-3093
940 **Giese H, Ackermann Jr, Heide H, Bleier L, DrÃ¶se S, Wittig I, Brandt U, Koch I** (2015) NOVA: a software
941 to analyze complexome profiling data. Bioinformatics **31:** 440-441
942 **Gray MW, Burger G, Lang BF** (1999) Mitochondrial evolution. Science **283:** 1476-1481
943 **Haslam TM, Feussner I** (2022) Diversity in sphingolipid metabolism across land plants. J Exp Bot **n:** doi:
944 10.1093/jxb/erab1558
945 **Haslam TM, Kunst L** (2013) Extending the story of very-long-chain fatty acid elongation. Plant Sci **210:** 93-
946 107
947 **Heilmann I** (2016) Phosphoinositide signaling in plant development. Development **143:** 2044-2055
948 **Hölzl G, Dörmann P** (2019) Chloroplast Lipids and Their Biosynthesis. Annu Rev Plant Biol **70:** null
949 **Hooper CM, Castleden IR, Tanz SK, Aryamanesh N, Millar AH** (2017) SUBA4: the interactive data analysis
950 centre for Arabidopsis subcellular protein locations. Nucleic Acids Research **45:** D1064-D1074
951 **Horvath SE, Daum G** (2013) Lipids of Mitochondria. Prog Lipid Res **52:** 590-614

952 **Inoue K** (2007) The chloroplast outer envelope membrane: the edge of light and excitement. Journal of
953 Integrative Plant Biology **49:** 1100-1111
954 **Inoue K** (2011) Emerging roles of the chloroplast outer envelope membrane. Trends Plant Sci **16:** 550-
955 557
956 **Jacoby RP, Li L, Huang S, Pong Lee C, Millar AH, Taylor NL** (2012) Mitochondrial composition, function
957 and stress response in plants. Journal of Integrative Plant Biology **54:** 887-906
958 **Jouhet J, Marechal E, Baldan B, Bligny R, Joyard J, Block MA** (2004) Phosphate deprivation induces
959 transfer of DGDG galactolipid from chloroplast to mitochondria. Journal of Cell Biology **167:** 863-
960 874
961 **Katayama K, Sakurai I, Wada H** (2004) Identification of an *Arabidopsis thaliana* gene for cardiolipin
962 synthase located in mitochondria. FEBS Lett **577:** 193-198
963 **Kim J, Na YJ, Park SJ, Baek S-H, Kim DH** (2019) Biogenesis of chloroplast outer envelope membrane
964 proteins. Plant Cell Rep **38:** 783-792
965 **Kitagaki H, Cowart LA, Matmati N, Vaena de Avalos S, Novgorodov SA, Zeidan YH, Bielawski J, Obeid**
966 **LM, Hannun YA** (2007) Isc1 regulates sphingolipid metabolism in yeast mitochondria. Biochim
967 Biophys Acta **1768:** 2849-2861
968 **Klahre U, Noguchi T, Fujioka S, Takatsuto S, Yokota T, Nomura T, Yoshida S, Chua NH** (1998) The
969 Arabidopsis *DIMINUTO/DWARF1* gene encodes a protein involved in steroid synthesis. Plant Cell
970 **10:** 1677-1690
971 **Lenarčič T, Albert I, Böhm H, Hodnik V, Pirc K, Zavec AB, Podobnik M, Pahovnik D, Žagar E, Pruitt R,**
972 **Greimel P, Yamaji-Hasegawa A, Kobayashi T, Zienkiewicz A, Gömann J, Mortimer JC, Fang L,**
973 **Mamode-Cassim A, Deleu M, Lins L, Oecking C, Feussner I, Mongrand S, Anderluh G,**
974 **Nürnberger T** (2017) Eudicot plant-specific sphingolipids determine host selectivity of microbial
975 NLP cytolysins. Science **358:** 1431-1434
976 **Li-Beisson Y, Shorrosh B, Beisson F, Andersson MX, Arondel V, Bates PD, Baud S, Bird D, DeBono A,**
977 **Durrett TP, Franke RB, Graham IA, Katayama K, Kelly AA, Larson T, Markham JE, Miquel M,**
978 **Molina I, Nishida I, Rowland O, Samuels L, Schmid KM, Wada H, Welti R, Xu C, Zallot R,**
979 **Ohlrogge J** (2013) Acyl-lipid metabolism. *In* C Somerville, E Meyerowitz, eds, The Arabidopsis
980 Book. The American Society of Plant Biologists, Rockville, MD, USA, p e0161
981 **Li L, Lavell A, Meng X, Berkowitz O, Selinski J, van de Meene A, Carrie C, Benning C, Whelan J, De Clercq**
982 **I, Wang Y** (2019) Arabidopsis DGD1 SUPPRESSOR1 is a subunit of the mitochondrial contact site
983 and cristae organizing system and affects mitochondrial biogenesis. Plant Cell **31:** 1856-1878

984 **Liebisch G, Fahy E, Aoki J, Dennis EA, Durand T, Ejsing C, Fedorova M, Feussner I, Griffiths WJ, Koefeler**
985 **H, Merrill AH, Murphy RC, O'Donnell VB, Oskolkova OV, Subramaniam S, Wakelam M, Spener F**
986 (2020) Update on LIPID MAPS classification, nomenclature and shorthand notation for MS-
987 derived lipid structures. J Lipid Res **61:** 1539–1555
988 **Mehrshahi P, Stefano G, Andaloro JM, Brandizzi F, Froehlich JE, DellaPenna D** (2013) Transorganellar
989 complementation redefines the biochemical continuity of endoplasmic reticulum and
990 chloroplasts. Proc Natl Acad Sci USA **110:** 12126-12131
991 **Michaud M, Gros V, Tardif M, Brugiere S, Ferro M, Prinz WA, Toulmay A, Mathur J, Wozny M, Falconet**
992 **D, Marechal E, Block MA, Jouhet J** (2016) AtMic60 is involved in plant mitochondria lipid
993 trafficking and is part of a large complex. Curr Biol **26:** 627-639
994 **Michaud M, Prinz WA, Jouhet J** (2017) Glycerolipid synthesis and lipid trafficking in plant mitochondria.
995 The FEBS Journal **284:** 376-390
996 **Miquel M, Browse J** (1992) *Arabidopsis* mutants deficient in polyunsaturated fatty acid synthesis. J Biol
997 Chem **267:** 1502-1509
998 **Mizoi J, Nakamura M, Nishida I** (2006) Defects in CTP:PHOSPHORYLETHANOLAMINE
999 CYTIDYLYLTRANSFERASE affect embryonic and postembryonic development in *Arabidopsis*. Plant
1000 Cell **18:** 3370-3385
1001 **Moreau F, Dupont J, Lance C** (1974) Phospholipid and fatty acid composition of outer and inner
1002 membranes of plant mitochondria. Biochim Biophys Acta **345:** 294-304
1003 **Morré DJ, Merritt WD, Lembi CA** (1971) Connections between mitochondria and endoplasmic reticulum
1004 in rat liver and onion stem. Protoplasma **73:** 43-49
1005 **Müller F, Frentzen M** (2001) Phosphatidylglycerophosphate synthases from *Arabidopsis thaliana*. FEBS
1006 Lett **509:** 298-302
1007 **Nandi A, Welti R, Shah J** (2004) The *Arabidopsis thaliana* dihydroxyacetone phosphate reductase gene
1008 *SUPPRESSOR OF FATTY ACID DESATURASE DEFICIENCY1* is required for glycerolipid metabolism
1009 and for the activation of systemic acquired resistance. Plant Cell **16:** 465–477
1010 **Nerlich A, von Orlow M, Rontein D, Hanson AD, Dörmann P** (2007) Deficiency in phosphatidylserine
1011 decarboxylase activity in the *psd*1 *psd*2 *psd*3 triple mutant of Arabidopsis affects
1012 phosphatidylethanolamine accumulation in mitochondria. Plant Physiol **144:** 904-914
1013 **Novgorodov SA, Wu BX, Gudz TI, Bielawski J, Ovchinnikova TV, Hannun YA, Obeid LM** (2011) Novel
1014 pathway of ceramide production in mitochondria. J Biol Chem **286:** 25352-25362

1015 **Quettier A-L, Shaw E, Eastmond PJ** (2008) SUGAR-DEPENDENT6 Encodes a Mitochondrial Flavin Adenine
1016 Dinucleotide-Dependent Glycerol-3-P Dehydrogenase, Which Is Required for Glycerol Catabolism
1017 and Postgerminative Seedling Growth in Arabidopsis. Plant Physiol **148:** 519-528
1018 **Rugen N, Straube H, Franken LE, Braun H-P, Eubel H** (2019) Complexome profiling reveals association of
1019 PPR proteins with ribosomes in the mitochondria of plants. Molecular & Cellular Proteomics **18:**
1020 1345-1362
1021 **Schaller H** (2003) The role of sterols in plant growth and development. Prog Lipid Res **42:** 163-175
1022 **Schikowsky C, Thal B, Braun H-P, Eubel H** (2018) Sample preparation for analysis of the plant
1023 mitochondrial membrane proteome. *In* H-P Mock, A Matros, K Witzel, eds, Plant Membrane
1024 Proteomics: Methods and Protocols. Springer New York, New York, NY, pp 163-183
1025 **Senkler J, Rugen N, Eubel H, Hegermann J, Braun H-P** (2018) Absence of complex I implicates
1026 rearrangement of the respiratory chain in european mistletoe. Curr Biol **28:** 1606-1613.e1604
1027 **Simm S, Papasotiriou D, Ibrahim M, Leisegang M, Müller B, Schorge T, Karas M, Mirus O, Sommer M,**
1028 **Schleiff E** (2013) Defining the core proteome of the chloroplast envelope membranes. Front
1029 Plant Sci **4**
1030 **Staehelin LA** (1997) The plant ER: a dynamic organelle composed of a large number of discrete functional
1031 domains. Plant J **11:** 1151-1165
1032 **Tarazona P, Feussner K, Feussner I** (2015) An enhanced plant lipidomics method based on multiplexed
1033 liquid chromatography–mass spectrometry reveals additional insights into cold- and drought-
1034 induced membrane remodeling. Plant J **84:** 621-633
1035 **Tatsuta T, Scharwey M, Langer T** (2014) Mitochondrial lipid trafficking. Trends Cell Biol **24:** 44-52
1036 **Tavassoli S, Chao JT, Young BP, Cox RC, Prinz WA, de Kroon AIPM, Loewen CJR** (2013) Plasma
1037 membrane - endoplasmic reticulum contact sites regulate phosphatidylcholine synthesis. EMBO
1038 rep **14:** 434-440
1039 **Thal B, Braun H-P, Eubel H** (2018) Proteomic analysis dissects the impact of nodulation and biological
1040 nitrogen fixation on *Vicia faba* root nodule physiology. Plant Mol Biol **97:** 233-251
1041 **Vance JE** (1990) Phospholipid synthesis in a membrane fraction associated with mitochondria. J Biol
1042 Chem **265:** 7248-7256
1043 **Watanabe M, Balazadeh S, Tohge T, Erban A, Giavalisco P, Kopka J, Mueller-Roeber B, Fernie AR,**
1044 **Hoefgen R** (2013) Comprehensive Dissection of Spatiotemporal Metabolic Shifts in Primary,
1045 Secondary, and Lipid Metabolism during Developmental Senescence in Arabidopsis. Plant Physiol
1046 **162:** 1290-1310

1047 **Wiedemann N, Pfanner N** (2017) Mitochondrial machineries for protein import and assembly. Annu Rev
1048 Biochem **86:** 685-714
1049 **Wittig I, Braun H-P, Schägger H** (2006) Blue native PAGE. Nat Protoc **1:** 418-428
1050 **Xu C, Hartel H, Wada H, Hagio M, Yu B, Eakin C, Benning C** (2002) The *pgp1* mutant locus of Arabidopsis
1051 encodes a phosphatidylglycerolphosphate synthase with impaired activity. Plant Physiol **129:**
1052 594-604
1053 **Xu Y, Malhotra A, Ren M, Schlame M** (2006) The enzymatic function of Tafazzin. J Biol Chem **281:** 39217-
1054 39224
1055 **Yamaoka Y, Yu Y, Mizoi J, Fujiki Y, Saito K, Nishijima M, Lee Y, Nishida I** (2011) *PHOSPHATIDYLSERINE*
1056 *SYNTHASE1* is required for microspore development in *Arabidopsis thaliana*. Plant J **67:** 648-661
1057 **Youn JH, Kim T-W, Joo S-H, Son S-H, Roh J, Kim S, Kim T-W, Kim S-K** (2018) Function and molecular
1058 regulation of DWARF1 as a C-24 reductase in brassinosteroid biosynthesis in Arabidopsis. J Exp
1059 Bot **69:** 1873-1886

1060